

## Critical Review

# Recent Advances in Understanding the Structure of Nicotinic Acetylcholine Receptors

Marios Zouridakis<sup>1,2</sup>, Paraskevi Zisimopoulou<sup>1</sup>, Konstantinos Poulas<sup>2</sup> and Socrates J. Tzartos<sup>1,2</sup>

<sup>1</sup>Department of Biochemistry, Hellenic Pasteur Institute, Athens, Greece

<sup>2</sup>Department of Pharmacy, University of Patras, Patras, Greece

### Summary

Nicotinic acetylcholine receptors (nAChRs), members of the Cys-loop ligand-gated ion channels (LGICs) superfamily, are involved in signal transduction upon binding of the neurotransmitter acetylcholine or exogenous ligands, such as nicotine. nAChRs are pentameric assemblies of homologous subunits surrounding a central pore that gates cation flux, and are expressed at the neuromuscular junction and in the nervous system and several nonneuronal cell types. The 17 known nAChR subunits assemble into a variety of pharmacologically distinct receptor subtypes. nAChRs are implicated in a range of physiological functions and pathophysiological conditions related to muscle contraction, learning and memory, reward, motor control, arousal, and analgesia, and therefore present an important target for drug research. Such studies would be greatly facilitated by knowledge of the high-resolution structure of the nAChR. Although this information is far from complete, important progress has been made mainly based on electron microscopy studies of *Torpedo* nAChR and the high-resolution X-ray crystal structures of the homologous molluscan acetylcholine-binding proteins, the extracellular domain of the mouse nAChR  $\alpha 1$  subunit, and two prokaryotic pentameric LGICs. Here, we review some of the latest advances in our understanding of nAChR structure and gating. © 2009 IUBMB

IUBMB *Life*, 61(4): 407–423, 2009

**Keywords** nicotinic acetylcholine receptors; membrane protein structure; ligand-binding; channel gating; drug design.

**Abbreviations** A-AChBP, *Aplysia californica* AChBP;  $\alpha$ -Btx,  $\alpha$ -bungarotoxin;  $\alpha$ -Cbtx,  $\alpha$ -cobratoxin;  $\alpha$ -Ctx,  $\alpha$ -conotoxin; ACh, acetylcholine; AChBP, acetylcholine-binding protein; CNS, central nervous system; ECD, extracellular domain; ELIC, prokaryotic ligand-gated ion channel

Received 30 August 2008; accepted 27 November 2008

Address correspondence to: Socrates J. Tzartos, Department of Biochemistry, Hellenic Pasteur Institute, GR11521 Athens, Greece or Department of Pharmacy, University of Patras, GR26500 Rio, Patras, Greece. Tel: +30-210-6478844 or +30-2610-969955. Fax: +30-210-6478842. E-mail: tzartos@pasteur.gr or tzartos@upatras.gr

ISSN 1521-6543 print/ISSN 1521-6551 online  
DOI: 10.1002/iub.170

from *Erwinia chrysanthemi*; EM, electron microscopy; GLIC, prokaryotic ligand-gated ion channel from *Gleobacter violaceus*; L-AChBP, *Lymnaea stagnalis* AChBP; LGIC, ligand-gated ion channel; M1–4, transmembrane segments 1–4; MIR, main immunogenic region; MG, myasthenia gravis; MLA, methyllycaconitine; nAChR, nicotinic acetylcholine receptor; nAChR-ECD, extracellular domain of the nAChR; TBS, transmitter binding site; TMD, transmembrane domain; TS, transition state.

### INTRODUCTION

Nicotinic acetylcholine receptors (nAChRs) belong to the superfamily of the Cys-loop ligand-gated ion channels (LGICs), which also includes the GABA, glycine, and 5-HT<sub>3</sub> receptors. The characteristic feature of this superfamily is a conserved sequence of 13 residues flanked by linked cysteines in the N-terminal domain of each subunit (*I*). The first nAChR subtype was purified from the electric organs of the fishes *Torpedo* and *Electrophorus*, and four types of subunits, namely,  $\alpha$ ,  $\beta$ ,  $\gamma$ , and  $\delta$ , were identified [reviewed in (2)]. The *Torpedo*  $\alpha$  subunit contains two adjacent linked cysteine residues (Cys192 and Cys193), which contribute to ligand binding; by convention, nAChR subunits with two adjacent cysteine residues at positions analogous to Cys192 and Cys193 in the *Torpedo*  $\alpha$  subunit are classified as  $\alpha$  subunits ( $\alpha 1$ – $\alpha 10$ ) (3).

In vertebrates, the 17 known homologous nAChR subunits ( $\alpha 1$ – $\alpha 10$ ,  $\beta 1$ – $\beta 4$ ,  $\gamma$ ,  $\delta$ , and  $\epsilon$ ) assemble into a variety of pharmacologically distinct receptor subtypes. The muscle nAChR is a heteropentamer, with a subunit stoichiometry of  $\alpha 1_2\beta 1\gamma\delta$  in the embryo, similar to that in *Torpedo* ( $\alpha 2\beta\gamma\delta$ ), whereas in adults, the  $\gamma$  subunit is replaced by the  $\epsilon$  subunit ( $\alpha 1_2\beta 1\epsilon\delta$ ). Muscle and *Torpedo* nAChRs are often named muscle-type nAChRs. The neuronal nAChR subtypes are also pentamers and are either homomers ( $\alpha 7$ ,  $\alpha 8$ ,  $\alpha 9$ , and  $\alpha 10$ ) or heteromers of  $\alpha$  and  $\beta$  subunits (e.g.,  $\alpha 4\beta 2$ ,  $\alpha 3\beta 4$ , and  $\alpha 4\alpha 2\beta 3$ ) but also of two different  $\alpha$  subunits (e.g.,  $\alpha 7\alpha 8$ ,  $\alpha 9\alpha 10$ ). The presence of a certain subunit can affect the localization, biophysical, functional, and

pharmacological properties of nAChRs and the regulation of the expression of the nAChR subtype at the developmental or adult stage, whereas the lack of a subunit may lead to the compensatory upregulation of other subtypes [reviewed in (4)].

Muscle-type nAChRs contain two ligand-binding sites for ACh and other cholinergic ligands, formed at the interfaces between an  $\alpha$  subunit and an adjacent  $\gamma/\epsilon$  or  $\delta$  subunit. The presence of different non- $\alpha$  subunits confers different affinities upon the two binding sites, resulted from intrinsic structural differences rather than from induced fit by the agonist (5). In neuronal nAChRs, the ligand-binding sites lie at the interface between two  $\alpha$  subunits in homomeric receptors or between an  $\alpha$  ( $\alpha 2$ ,  $\alpha 3$ ,  $\alpha 4$ , or  $\alpha 6$ ) and a  $\beta$  ( $\beta 2$  or  $\beta 4$ ) subunit in heteromeric receptors. The  $\alpha 5$  and  $\beta 3$  subunits do not participate in the formation of ligand-binding sites, but may contribute to nAChR targeting and localization in neuronal plasma membrane domains (6, 7).

Muscle-type nAChRs are located postsynaptically at the neuromuscular junction, where they mediate fast chemical transmissions of electrical signals from invading motor neurons. Neuronal nAChRs are expressed widely in the central nervous system (CNS) and peripheral nervous system, where they are distributed post-, pre-, and/or perisynaptically (8). When neuronal nAChRs are expressed on presynaptic membranes, their activation is involved in the modulation of synaptic transmission by the release of ACh, noradrenaline, dopamine, glutamate, and GABA; when expressed on postsynaptic membranes, their activation triggers intracellular signaling mechanisms for cell excitability, gene expression, cell differentiation and survival. Neuronal nAChRs have also been found in nonneuronal cells, such as endocrine, endothelial, epithelial, and immune system cells (9), and have also been identified in insects and other invertebrates, representing targets for neuroactive pesticides (10).

Binding of ACh, or other cholinergic agonists, to nAChRs triggers a reversible process, called gating, which renders them permeable to  $\text{Na}^+$ ,  $\text{K}^+$ , and in some neuronal subtypes (e.g., in the homomeric  $\alpha 7$  nAChR),  $\text{Ca}^{2+}$  ions (11). This process results in the depolarization of the cell membrane where these nAChRs are located, and the subsequent modulation of neuronal activity or muscle contraction. It should be noted that the nAChRs are allosteric proteins and can adopt three different states or conformations; (a) a closed or resting state, which is a nonconducting and low-affinity state for binding of agonists, (b) an open state, which is a conducting and high-affinity state for agonist binding, and (c) a desensitized state, which is a nonconducting but high-affinity agonist binding state. Regarding the allosteric states of nAChR, binding of ACh or other agonists to nAChRs triggers their transition from the closed to the open state, whereas prolonged exposure of nAChRs to agonists leads to their desensitized state and termination of the cation flux through the nAChR channel. After removal of the agonist, nAChRs recover back to their initial resting state.

The diversity of nAChR subtypes, localization, and function is the reason for their involvement in several pathological con-

ditions. The most common acquired disorder, implicating muscle nAChR, is myasthenia gravis (MG), an autoimmune disease in which the muscle nAChR is the target of autoantibodies in the majority of affected patients. The hallmark feature of MG is fluctuating muscle weakness. In MG, most of the pathogenic autoantibodies target a specific region of nAChR  $\alpha 1$  subunit, known as the “main immunogenic region” (MIR) (12, 13). Autoantibodies bound to the MIR are perfectly oriented to cross-link adjacent nAChRs, triggering an increase in the rate of nAChR internalization and degradation (13, 14). The congenital myasthenic syndromes are genetic disorders of the neuromuscular junction and are usually due to mutations that reduce the expression or alter the kinetics of the muscle nAChR (15, 16).

Neuronal nAChRs are implicated in the pathogenesis of several diseases of the CNS. Diseases due to mutations of nAChR subunit genes and subsequent alteration of receptor function have been described, for example, autosomal dominant frontal lobe epilepsy mutations in the channel region of the  $\alpha 4$  or  $\beta 2$  subunits (17, 18). More importantly, some diseases, such as schizophrenia, Tourette’s syndrome, attention-deficit hyperactivity disorder, autism, depression, anxiety, and the neurodegenerative Alzheimer’s and Parkinson’s diseases, are associated with altered numbers of nAChR subtypes. nAChRs are also responsible for tobacco dependence and behavioral effects of nicotine [reviewed in (4, 19)].

To design drugs with minimum side effects and specifically targeting single nAChR subtypes to treat the above mentioned diseases, detailed structural information on the various nAChR subtypes and their complexes with ligands is needed. Significant efforts have been made in the last few years, and our knowledge regarding nAChR structure and its relation to function has been dramatically increased by the determination of (a) the X-ray crystal structures, at up to 1.76 Å resolution, of the ligand-free or ligand-bound molluscan ACh-binding proteins (AChBPs), which are soluble protein homologues of the extracellular domains (ECDs) of nAChRs (20–27), (b) the 4 Å resolution electron microscopy (EM) structure of the *Torpedo* nAChR (28), (c) the X-ray crystal structure at 1.94 Å resolution of the mouse nAChR  $\alpha 1$ -ECD bound to  $\alpha$ -bungarotoxin ( $\alpha$ -Btx) (29), and (d) the X-ray crystal structures of two prokaryotic LGICs; one from the bacterium *Erwinia chrysanthemi* (ELIC protein), resolved at 3.3 Å resolution (30) and another one from the bacterium *Gleobacter violaceus* (GLIC protein), which was resolved coinstantaneously by two different groups at 3.1 (31) and 2.9 Å (32) resolution, respectively.

## OVERVIEW OF nAChR STRUCTURE

Early structural information on nAChRs was derived from EM studies on two-dimensional arrays of the *Torpedo* nAChR in its closed and open states (33, 34), which revealed the dimensions and shape of the molecule, the location of the ligand-binding sites, and the organization of the ion channel.

The first milestone in understanding the structure of nAChRs in atomic detail was the elucidation of the **X-ray crystal structure of the molluscan *Lymnaea stagnalis* AChBP (L-AChBP) at 2.7 Å resolution (20)**. This protein, a soluble homopentamer of a 210 amino acid subunit, aligns well with the ECDs of all LGICs (20), showing the greatest similarity with nAChR-ECDs (up to 24%), binds nAChR ligands (35), and, when attached to the pore domain of the 5-HT<sub>3A</sub> receptor, leads to the opening of this hybrid channel on ACh binding (36). The AChBP is therefore a structural and functional homologue of nAChR-ECDs and serves as a model for their study. Like the nAChRs, AChBP assembles into a homopentamer with ligand-binding characteristics that are typical for a nicotinic receptor; unlike the nAChRs, however, it lacks the domains to form a transmembrane ion channel. Therefore, any comparison made in this text between AChBP and nAChR implicates only the ECDs of nAChR. AChBP differs in function from the nAChRs, as it plays a modulatory role in molluscan synaptic transmission (35, 37). More specifically, in response to the accumulating concentrations of the presynaptically released ACh into the molluscan synaptic cleft under conditions of active neurotransmission, AChBP is secreted from perisynaptic glial cells to the cleft and captures ACh molecules, therefore diminishing or terminating synaptic transmission (37). AChBP is released to the synaptic cleft after binding of ACh to nAChRs present on the perisynaptic glial cells. So far, no orthologs of AChBP have been found in other animal phyla.

The resolved dimensions of the AChBP (a 62 Å high cylinder, with a diameter of 80 Å and a central 18 Å diameter hole) (20) are in good agreement with those estimated for the *Torpedo* nAChR-ECD by EM studies (38, 39). When viewed along the fivefold axis, the AChBP resembles a toy windmill, with blade-like monomers (Fig. 1A). Each monomer consists of an N-terminal  $\alpha$ -helix, two short  $3_{10}$  helices, and a  $\beta$ -sandwich hydrophobic core consisting of 10  $\beta$ -strands ( $\beta 1$ – $\beta 10$ ), connected by an equal number of loops and arranged in two sets joined through a cysteine bridge, the Cys-loop (Fig. 1B). However, in the Cys-loop of AChBP, the cysteines are spaced by only 12 instead of the 13 amino acid residues in the corresponding Cys-loop regions of LGICs, whereas there is no sequence conservation between these loop regions of AChBP and LGICs.

The structure of the AChBP and a subsequent 4 Å resolution EM study of the *Torpedo* nAChR (28) were used to create the refined 4 Å model of the whole receptor in its closed state (28). In this model, which constitutes the second milestone in our understanding of nAChR structure in atomic detail, the receptor was shown to have a total length of  $\sim 160$  Å normal to the membrane plane and to be divided in three domains: (a) an N-terminal ECD, or ligand-binding domain, which shapes a  $\sim 60$  Å long central vestibule with a diameter of  $\sim 20$  Å, and has two binding sites for ACh, (b) a transmembrane domain (TMD), components of which form a  $\sim 40$  Å long water-filled narrow pore, containing the gate of the channel, (c) an intracellular domain, which shapes a smaller vestibule than the extracellular

one and which has narrow lateral openings for the ions, and (d) a short C-terminal extracellular tail (Figs. 2B and 2C). The subunits of the *Torpedo* nAChR all have a similar size (maximum dimensions 30 Å  $\times$  40 Å  $\times$  160 Å) and the same three-dimensional fold (28).

### Extracellular Domain

The nAChR-ECDs are each organized around a hydrophobic core of 10  $\beta$ -strands, joined through the Cys-loop, and contain one N-terminal  $\alpha$ -helix (28), like the AChBP protomer (20). These domains also contain several loop regions that are critical for receptor function, such as loops A, B, and C, the Cys-loop, and the  $\beta 1$ – $\beta 2$  loop (Fig. 2C). The 4 Å EM structure of the *Torpedo* nAChR showed that the two ACh-binding sites of the receptor are shaped by loops A, B, and C of the  $\alpha$  subunit and several structural elements of the adjacent  $\gamma$  or  $\delta$  subunit, and that these sites lie about 40 Å above the membrane surface on opposite sides of the channel pore (Fig. 2A) (28). These findings confirmed the results of earlier mutagenesis and affinity-labeling studies indicating that two separate parts of the nAChR-ECD are involved in the formation of the ACh-binding site (40–42). One is called the “principal component” or plus side of the binding site, involving loops A, B, and C of the  $\alpha$  subunit, whereas the other is called the “complementary component” or minus side, formed by loops D, E, and F of the adjacent non- $\alpha$  subunit ( $\gamma$  or  $\delta$  subunit).

The *Torpedo* nAChR-ECDs interact mainly through polar side chains (28). The interfaces on both sides of the  $\alpha$ -ECDs contain amino acid residues with charged side chains, which form ion pairs with oppositely charged side chains of residues on neighbouring subunits. These interactions may be important for the special conformation of the  $\alpha$  subunits in the resting state of the nAChR, which is discussed later. Notably, there are no equivalent electrostatic interactions between charged side chains at the  $\beta$ – $\delta$  (non- $\alpha$ ) interface. The narrow interstitial spaces left between the contact areas on the subunit interfaces in the ECD form a  $\sim 20$  Å wide extracellular vestibule, through which ions flow because of their electrochemical gradient when the channel opens. The inner wall of the extracellular vestibule is lined by an excess of negatively charged amino acid residues (residues Glu13, Asp44, Glu51, Asp71 on  $\alpha$  subunits, Asp residues at sites 84, 89, 97 and Glu residues at sites 45, 82, 100 of the  $\beta$  subunit, Glu residues at sites 82 and 100 of the  $\gamma$  subunit, and Asp49 on the  $\delta$  subunit), promoting a cation-stabilizing environment (28). Therefore, this vestibule is selectively permeable to diffusing cations.

The MIR, a region of overlapping epitopes, was first identified in the *Torpedo*  $\alpha$ -ECD; in the autoimmune MG disease, a large fraction of the anti-nAChR autoantibodies are directed against the corresponding region of the human  $\alpha 1$ -ECD (43, 44). A critical segment of the MIR forming the main part of the epitope for some anti-MIR monoclonal antibodies was localized to residues  $\alpha$ Trp67– $\alpha$ Asp76, with  $\alpha$ Asn68 and  $\alpha$ Asp71 being the

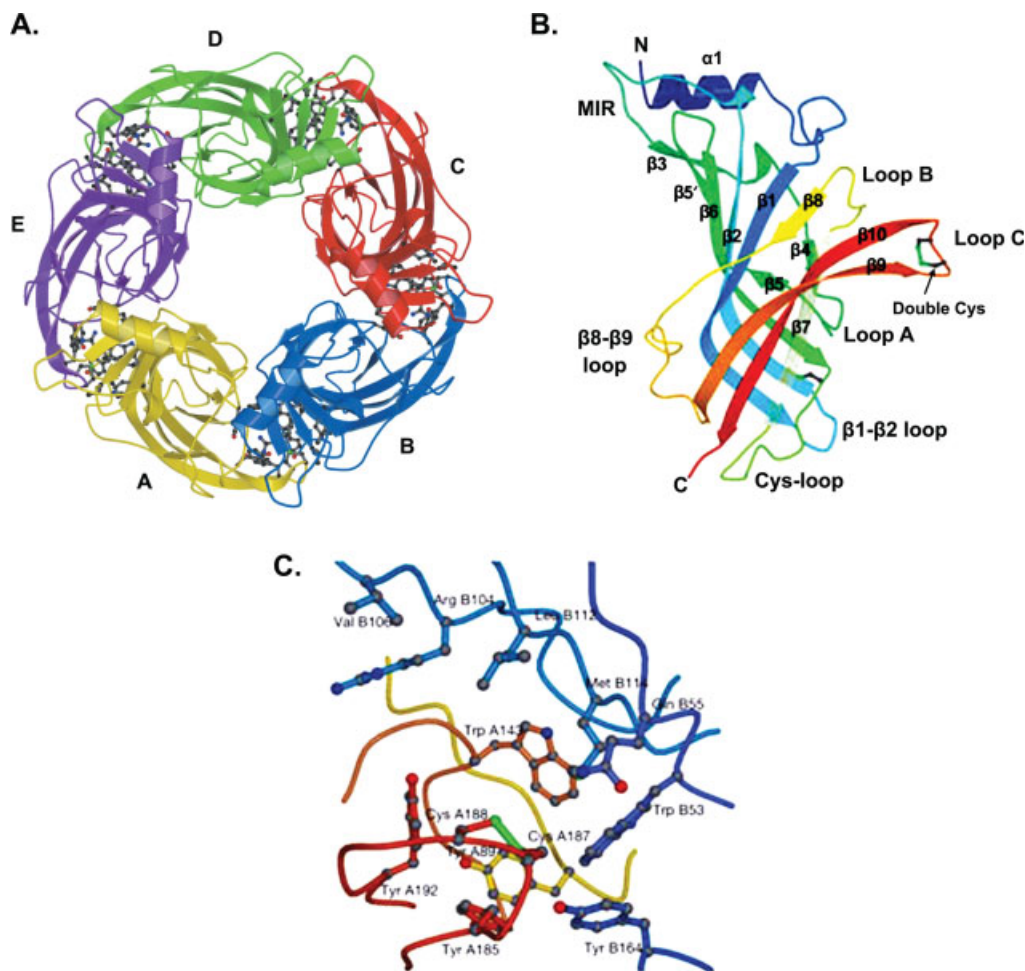


**Figure 1.** Crystal structure of *Lymnaea stagnalis* AChBP, a homologue of nAChR-ECDs. (A) Top view. Each subunit of the homopentamer is shown in a different color and indicated by a different letter (A–E). The ligand-binding sites at the interfaces of the subunits are shown in ball-and-stick representation. (B) Side view of the L-AChBP protomer from outside the pentameric ring. The side of the protomer bearing the Cys-loop is called the principal or plus side. Also shown are the 10  $\beta$ -strands ( $\beta$ 1–10) constituting the hydrophobic core of the protomer; the N-terminal  $\alpha$ -helix; loops A, B, and C which contribute to the formation of the principal side of the ligand-binding sites; loops  $\beta$ 1– $\beta$ 2 and  $\beta$ 8– $\beta$ 9; the Cys-loop; and the region corresponding to the MIR epitope of the muscle nAChR  $\alpha$ 1 subunit. (C) Ball-and-stick representation of the AChBP ligand-binding site, showing the contribution of residues in the principal loops A (yellow), B (dark yellow), and C (orange) and residues in the complementary loops D (violet), E (light blue), and F (blue). Reproduced with permission from Brejc et al., Nature, 2001, 411, 269–276.

most important (43, 45). These residues appear to be exposed to the solvent in the *Torpedo* nAChR EM structure (Fig. 2), contrasting with the equivalent regions of the non- $\alpha$  subunits, which are partially buried by the respective N-terminal  $\alpha$ -helices (28). The third milestone in structural information on nAChRs in atomic detail, the X-ray crystal structure of the mouse nAChR  $\alpha$ 1-ECD complexed with  $\alpha$ -Btx (29), confirmed that the MIR is located at a protruding and highly accessible point near the N-terminal  $\alpha$ -helix (Fig. 3A) and showed that its conformation is maintained by interactions (mainly hydrogen bonds and van der Waals contacts) between this helix, the  $\beta$ 5– $\beta$ 6 turn of the hydrophobic core, and a  $3_{10}$ -helix (Fig. 3B).

The fourth milestone in the structural study of nAChRs was the X-ray crystal structure of ELIC (Fig. 4) (30) and more recently of GLIC (31, 32), two prokaryotic pentameric LGICs, which are cation-selective channels and considered to be the ancestors of nAChRs (46). ELIC-ECD (Fig. 4B) (30) and GLIC-ECD (31, 32) have both similar structure with the AChBP and the *Torpedo* nAChR-ECDs, but lack the N-terminal  $\alpha$ -helix and the Cys-loop.

CD studies on the human muscle  $\alpha$ 1-,  $\beta$ 1-,  $\gamma$ -, and  $\delta$ -ECDs and neuronal  $\alpha$ 7-ECD expressed in the yeast *Pichia pastoris* (47) have shown that the secondary structural composition of these domains ( $\sim$ 45%  $\beta$ -sheet and  $\sim$ 5%  $\alpha$ -helix)

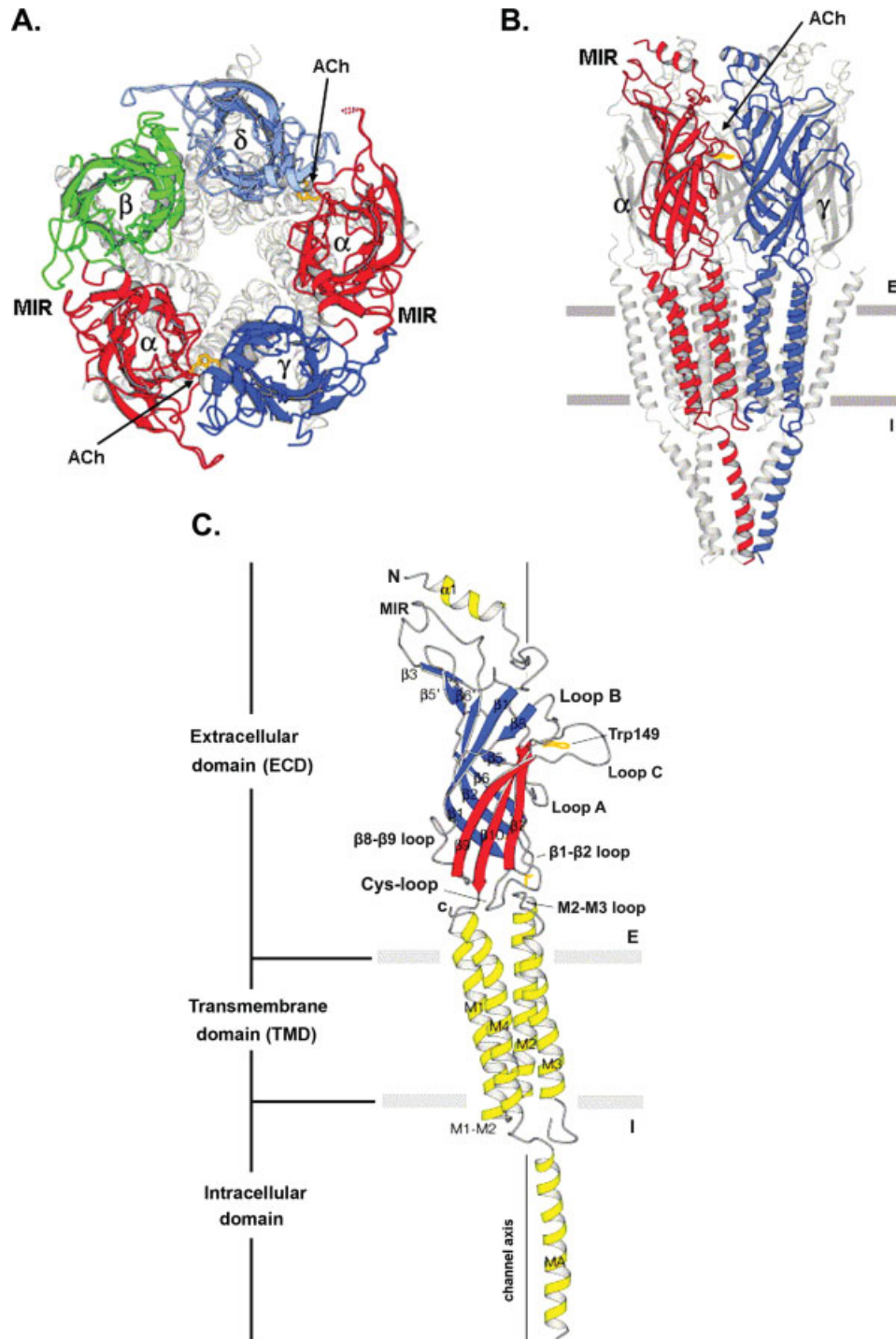


**Figure 2.** Electron microscopy structure of the *Torpedo* nAChR. Ribbon diagrams of the whole nAChR as viewed (A) from the synaptic cleft and (B) parallel to the membrane plane. The locations of the ACh-binding sites, the side chain of the highly conserved  $\alpha$ Trp149 residue (gold) in the principal side of the ligand-binding site, and the MIR epitope of the  $\alpha$  subunit are shown. (C) Ribbon diagram of the side-view of the  $\alpha$  subunit in an orientation with the central axis of the pentamer at the back. Loops A, B, and C form the principal side of the ACh-binding site, and  $\beta 1$ - $\beta 2$  loop and the Cys-loop are in contact with the M2-M3 loop of the TMD, thus coupling the conformational changes occurring in the ECD on binding of ACh or other nAChR agonists to the TMD. (Cell membrane: between the horizontal bars; E: extracellular; I: intracellular). Reproduced with permission from Unwin, J. Mol. Biol., 2005, 346, 967–989.

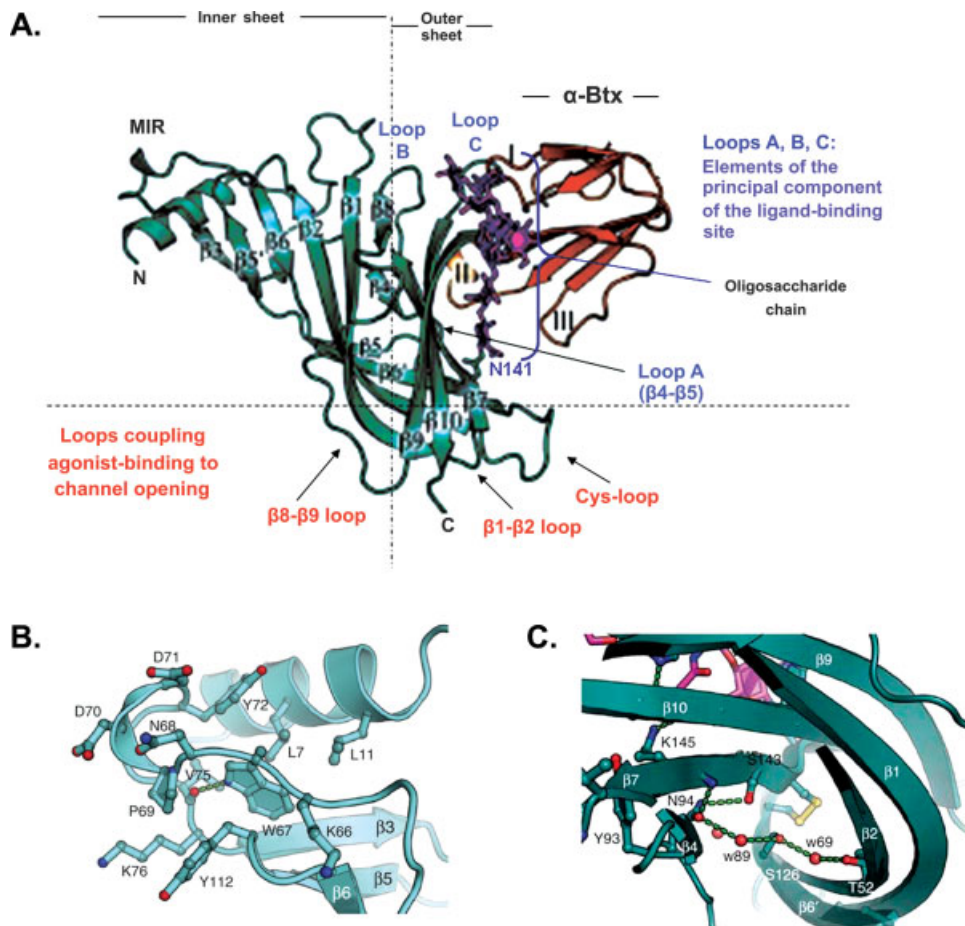


**Figure 3.** Crystal structure of mouse nAChR  $\alpha 1$ -ECD bound to  $\alpha$ -Btx. (A) This scheme represents the front view of the  $\alpha 1$ -ECD between the inner ( $\beta 1$ – $\beta 3$ ,  $\beta 5$ ,  $\beta 6$ ,  $\beta 8$ ) and outer ( $\beta 4$ ,  $\beta 7$ ,  $\beta 9$ ,  $\beta 10$ )  $\beta$ -sheets of the hydrophobic core of the protein. The  $\alpha 1$ -ECD,  $\alpha$ -Btx, and the oligosaccharide chain linked to Asn141 (N141) of the  $\alpha 1$ -ECD are shown in cyan, orange, and magenta, respectively. (B) Atomic structure of the main epitope of the MIR (residues 66–76 of the  $\alpha 1$ -ECD), showing its interactions with the N-terminal  $\alpha$ -helix and the  $\beta 5$ – $\beta 6$  turn of the  $\alpha 1$ -ECD. (C) A detailed view from the top of the  $\beta$ -barrel of  $\alpha 1$ -ECD, showing the pathway in the hydration cavity formed by a chain of water molecules hydrogen-bonded to Thr52 (T52) and Ser126 (S126) in the inner  $\beta$ -sheets ( $\beta 2$  and  $\beta 6'$  strands, respectively) and Asn94 (N94) in loop A. Water molecules are represented as red balls. Reproduced with permission from Dellisanti et al., *Nat. Neurosci.*, 2007, 10, 953–962.

is conserved and similar to that of the *Torpedo*  $\alpha$ -ECD (28).

### Transmembrane Domain

The TMD of each nAChR subunit is made up of four membrane-spanning  $\alpha$ -helical domains (M1–M4) (Fig. 2C) (28). The M2  $\alpha$ -helices of all five subunits are 40 Å long and shape the central conduction path, whereas the M1, M3, and M4  $\alpha$ -helices coil around each other and form an outer ring, shielding the inner ring of the M2 domains from the membrane lipids. In the TMD, the responsible amino acid residues for the subunit–subunit contacts are hydrophobic, with their side chains projecting away from the helices M1, M2, and M3 (39). The M2 helices from all subunits traverse the membrane in register with sets of

homologous residues at each level, forming rings of chemically distinct environments facing the lumen of the pore. The majority of these rings are nonpolar. However, there is an interaction involving the negatively charged Glu262 residues of the  $\alpha$  subunits (near the end of M2 helix) with the positively charged Arg277 and Lys271 residues on  $\delta$  and  $\gamma$  subunits, respectively, forming the “extracellular ring.” This ring, together with another one at  $\alpha$ Ser266, which also involves a negatively charged group, is expected to influence ion transport when the channel is open by facilitating the transport of cations at the extracellular entrance of the membrane-spanning pore. There is also a negatively charged third ring at  $\alpha$ Glu241, the “intermediate ring,” formed slightly beyond the intracellular ends of the M2 helices, framing the intracellular entry of the pore (39).

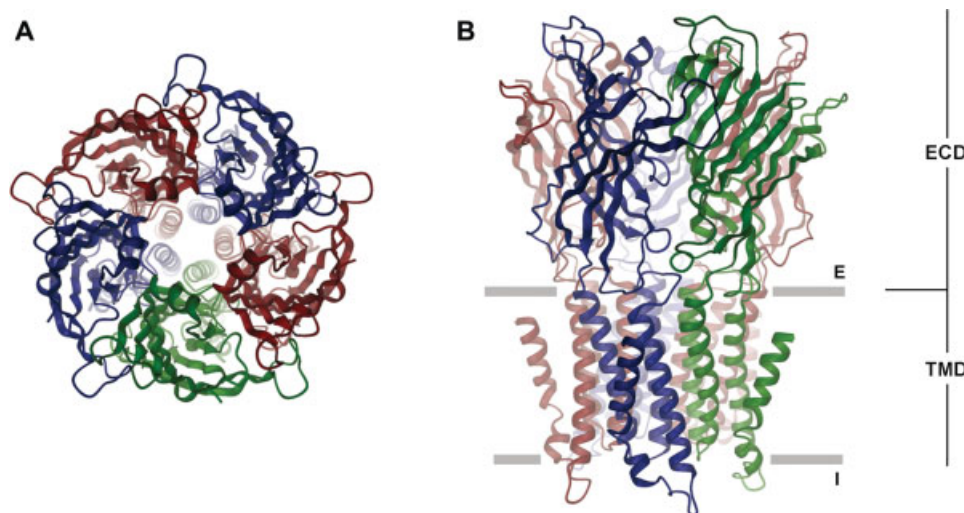


**Figure 4.** Crystal structure of the ELIC, a prokaryotic LGIC. Structure of the pentameric channel as viewed from (A) the extracellular side and perpendicular to the membrane plane, showing the four  $\alpha 2$  helices from each subunit forming the channel pore, and (B) from the side, parallel to the membrane plane. The subunits of the ELIC lack the N-terminal  $\alpha$ -helix, Cys-loop, and cytoplasmic loop of the eukaryotic LGICs. (Cell membrane: between the horizontal bars; E: extracellular; I: intracellular). Reproduced with permission from Hilf and Dutzler, *Nature*, 2008, 452, 375–379.

In the closed channel, the M2  $\alpha$ -helices tilt inward toward the central axis until they reach the middle of the membrane, where they come together and make a tight hydrophobic girdle around the pore, which is the narrowest region of the channel pore (28). This hydrophobic girdle constitutes the gate of the channel and functions as an energetic barrier to ion permeation, as its  $\sim 6$  Å diameter is too constricting for a hydrated sodium or potassium ion to pass through, given that the ion cannot readily lose part of its hydration shell in the absence of polar surfaces that would substitute for water (28). The major components of the gate of the *Torpedo* nAChR channel are  $\alpha$ Leu251 (9' residue of  $\alpha$ M2) and  $\alpha$ Val255 (13' residue of  $\alpha$ M2) residues, which make hydrophobic contacts with a neighbouring Ala (or Ser) or with a neighbouring Phe residue, respectively (39, 48).

The structure of the prokaryotic ELIC-TMD (Fig. 4) (30) and GLIC-TMD (31, 32) is similar to that of the *Torpedo* nAChR-TMD (28), as it consists of four  $\alpha$ -helices ( $\alpha 1$ – $\alpha 4$ ), equivalent to the M1–M4 transmembrane regions of the *Torpedo* nAChR. These helices from all five subunits are arranged in two concentric layers around the pore axis; an inner circle formed by the  $\alpha 2$  helices shapes the pore (Fig. 4A), which is shielded and stabilized by an outer circle of helices  $\alpha 1$  and  $\alpha 3$ . Although there are differences in the diameter of the pore between the bacterial and eukaryotic LGICs, the hydrophobic environment at the membrane centre and the presence of negatively charged residues at the periphery of the channel, which confers ion selectivity, are preserved (30–32). It should be noticed that the structure of ELIC represents the closed state of the prokaryotic LGICs (30). The gate appears to be formed by the contribution of three hydrophobic bulky residues (Leu239,

Ala243, and Phe246), which point their side chains toward the central axis, creating a hydrophobic barrier of a diameter of 2 Å to ion permeation. Interestingly, residues Leu239 and Ala243 are at equivalent positions on the  $\alpha 2$ -helices of ELIC-TMD with the homologous gate-defining residues  $\alpha$ Leu251 and  $\alpha$ Val255 on the *Torpedo* M2-helices.

Notably, the most recently published, from two different groups, structure of GLIC, a proton-gated LGIC, represents the open state of the prokaryotic LGICs (31, 32). The structure of GLIC revealed a different conformation in the pore region of the channel compared with that observed in ELIC. Briefly, although the transmembrane pore of ELIC is constricted on its extracellular side (30), the equivalent region of GLIC presents a funnel-shaped opening with a linearly decreasing diameter, placing its narrowest part at the intracellular entry of the channel (31, 32). More specifically, the pore of GLIC has a diameter of 12 and 5 Å toward the extracellular and the intracellular ends of M2-helices, respectively, in contrast with the diameters of 2 and 10 Å of the respective regions of ELIC. The wide opening from 2 to 12 Å of the GLIC region where the gate of the channel is located leads to the ion permeability of the GLIC channel, because there is no more a hydrophobic barrier to the ion flux through the pore. Comparison of the structures of GLIC (open channel) and ELIC (closed channel) propose a gating mechanism for the prokaryotic LGICs, which may plausibly be extended to eukaryotic LGICs (31, 32).

### Intracellular Domain

The nAChR intracellular region consists of a large cytoplasmic loop, the M3–M4 loop, which varies in length between the

different subunits (110–270 amino acid residues) and contains a curved  $\alpha$ -helix (MA) prior to the M4 helix (Fig. 2C) (28). Most of the loop immediately after the M3 helix (M3-MA loop) seems to be disordered and was not resolved in the 4 Å EM structure. Structural studies of the *Torpedo californica* and rat  $\delta$ M3-M4, involving CD spectroscopy and NMR, also suggested that most of this loop is unordered (49, 50). However, it has been demonstrated that structural disorder is important to the functions of some proteins (51), and in this case, it might contribute to the various functions of the large nAChR cytoplasmic loops in the resting, open, and desensitized states.

The MA  $\alpha$ -helices of all five subunits shape the wall of the intracellular vestibule, which similarly to the extracellular vestibule is  $\sim 20$  Å wide, and also lined by negatively charged amino acid residues (Glu residues at sites 390, 397, and 398 of the  $\alpha$  subunits, residues Glu423 and Asp427 on the  $\beta$  subunit, and Glu437 on the  $\gamma$  subunit), promoting a cation-stabilizing environment (28). The MA helices from each subunit together create an inverted pentagonal cone (Fig. 2B), having five intervening spaces (“windows”) less than 8 Å wide (comparable to the diameter of a hydrated sodium or a potassium ion), surrounded by negatively charged side-chains. These “windows” facilitate the transport of small cations, but prevent the passage of anions and large ions, and together with the extracellular and intracellular vestibules constitute the charge and size “selectivity filter” of the nAChR channel (28).

The large cytoplasmic loop of each nAChR subunit contains unique sequences that are distinguishing fingerprints for each subunit. It has been demonstrated that residues in the large cytoplasmic loop near the intracellular end of M4 affect the assembly of subunits and electrophysiological properties of nAChRs (52–55). These loops have been suggested to play potential roles in the regulation of nAChR trafficking (56–61) and in interactions with the cytoskeleton (52, 62–66), which induce nAChR clustering. In addition, several phosphorylation sites have been found in the cytoplasmic loop (67, 68), whose phosphorylation affects desensitization (69, 70), expression (71, 72), and interactions with cytoskeleton (73). Palmitoylation (74, 75) of the cytoplasmic loop of  $\alpha 7$  nAChR has been shown to affect the expression of this subtype receptor (76). Apparently, to fully understand how nAChRs work, further insight into the structure of the M3–M4 loop and its posttranslational modifications and interactions with other proteins is needed.

Notably, the bacterial LGICs lack the intracellular M3–M4 loop (Fig. 4B) (30–32, 46), which has probably developed to fulfill specific functions of the nAChR, such as ion permeation and protein clustering via interactions with rapsyn (64, 66).

## ATOMIC STRUCTURE OF THE nAChR LIGAND-BINDING SITE

Our knowledge of the atomic structure of the nAChR ligand-binding site is mainly due to the determination of the high-resolution X-ray crystal structures of various molluscan

AChBPs. In the first crystal structure of the L-AChBP (20), it was shown that each ligand-binding site, formed at the interfaces between the five subunits (Fig. 1A), is lined by conserved aromatic and hydrophobic aromatic amino acids from disperse regions of the protein, which help to form an aromatic pocket that binds quaternary ammonium compounds through cation- $\pi$  interactions. More specifically, the ligand-binding site is formed by residues from loops A (Tyr89), B (Trp143 and Trp145), and C (Tyr185, the double cysteine 187–188, and Tyr192) in the plus side of one subunit, which are highly conserved throughout the LGIC superfamily, and by less conserved residues from loops D (Trp53 and Gln55), E (Arg104, Val116, Leu112, and Met114), and F (Tyr164) in the minus side of the adjacent subunit (Fig. 1C). The plus side of each subunit is the one bearing the Cys-loop when the AChBP monomer is viewed from the side and perpendicular to the fivefold axis (Fig. 1B). The HEPES molecule used in the crystallization buffer mimics cholinergic ligands, as it contains a positively charged quaternary ammonium group, and was found to be stacked by cation- $\pi$  interactions on the highly conserved Trp143 [equivalent to  $\alpha$ Trp149 in *Torpedo* (see Fig. 2C)] in each ligand-binding site, thus revealing the critical role of Trp143 in this process (20). The HEPES-L-AChBP complex is believed to represent the structure of the nAChR-ECD in its desensitized state (77).

The subsequent solution of the crystal structure of the mouse nAChR  $\alpha 1$ -ECD (29) revealed the same structure for at least the principal side of the ligand-binding site (Fig. 3A), thus validating the use of the preceding structures of the AChBP in drug design. Interestingly, several of the aromatic residues involved in the formation of the nAChR ligand-binding site are also present in the prokaryotic LGIC-ECDs, despite the fact that the ligand might be as small as a proton in these bacterial proteins (30–32).

## Agonist Binding

The crystal structures of the L-AChBP complexed with nicotine or carbamylcholine (21) and the *Aplysia californica* AChBP (A-AChBP) complexed with lobeline or epibatidine (22) revealed the interactions between agonists and LGICs at the atomic scale. In all agonist-bound AChBP structures, the agonist is fully enveloped by the protein, through hydrogen bonds and  $\pi$ -cation, dipole-cation, and van der Waals forces with residues, especially of loop C. A highly conserved Trp143 (L-AChBP numbering) from the principal face of the subunit (Fig. 1C) makes strong aromatic  $\pi$ -cation interactions with all four agonists. The vicinal cysteine residues in loop C (Figs. 1B and 1C) make contacts with each of the above agonists, mostly involving Cys187 in the case of carbamylcholine and Cys188 in the case of nicotine (L-AChBP numbering). In all cases, agonist binding is supported by interactions with residues of the less conserved minus face, conferring ligand-binding specificity.

### Antagonist Binding

Snake neurotoxins and snail conotoxins have been used for the isolation and biochemical characterization of nAChRs, as they are competitive antagonists of the nAChR. Using synthetic peptides,  $\alpha$ -neurotoxin-binding sites have been identified on both neuronal and muscle  $\alpha$  subunits (78–81). Specifically, our group showed that the main  $\alpha$ -Bgtx-binding segment corresponds to residues 189–195 in the *Torpedo*  $\alpha$  (79) and to 186–197 in the human  $\alpha 7$  nAChR subunit (81).

The crystal structures of the complexes of L-AChBP with  $\alpha$ -cobratoxin ( $\alpha$ -Cbtx) (25), A-AChBP with  $\alpha$ -conotoxins ( $\alpha$ -Ctxs) (22, 23, 26, 27), mouse nAChR  $\alpha 1$ -ECD with  $\alpha$ -Btx (29), and A-AChBP with the small alkaloid antagonist methyllycaconitine (MLA) (22) identified the residues involved in toxin/antagonist binding in atomic detail. These structures showed that the binding of competitive antagonists involves interactions through extensive hydrogen bonds and van der Waals contacts with highly conserved amino acids in the principal side of the ligand-binding pockets, especially residues in loop C, and interactions with various less conserved amino acids in the complementary side of the binding pocket, most of which belong to loop F. A noticeable difference with the agonist-bound AChBP structures (21, 22) is that loop C in the antagonist-bound AChBPs (22, 23, 25–27) and mouse  $\alpha 1$ -ECD (29) does not envelop the antagonists.

Furthermore, the structure of the mouse  $\alpha 1$ -ECD (29) also revealed the fine ordering of a glycan chain linked to Asn141 (the penultimate amino acid residue of the Cys-loop) (Fig. 3A) and the important role of glycosylation of the nAChR  $\alpha 1$  subunit in  $\alpha$ -Btx-binding, confirming the results of earlier biochemical studies (82). However, glycosylation does not seem to be essential for  $\alpha$ -Btx binding to the neuronal  $\alpha 7$ -ECD, as the deglycosylated and glycosylated proteins bind  $\alpha$ -Btx with the same binding affinity (83).

### Allosteric Ligand Binding

Apart from the ACh-binding site, also called the nAChR orthosteric binding site, other allosteric binding sites have been identified on nAChRs (84–86). These modulate channel activity by binding ligands that do not compete with ACh or  $\alpha$ -Btx and which are either positive or negative allosteric modulators, increasing or decreasing agonist-induced activity, respectively. These allosteric ligand-binding sites have been shown to be located in the ion pore (channel blockers) or the extracellular, cytoplasmic, and transmembrane domains (Fig. 5).

The recently resolved X-ray crystal structures for the complexes of the A-AChBP with the noncompetitive nAChR ligands galanthamine [positive allosteric modulator (87)] and cocaine [negative allosteric modulator (88, 89)] (90) show that these ligands bind deep within the subunit interfaces of the AChBP, but, in contrast to competitive nAChR ligands, do not interact with the tip of loop C. Furthermore, because the amino acid residues of the AChBP that make contact with cocaine and

galanthamine are conserved in neuronal non- $\alpha$  subunits, the equivalent sites at which noncompetitive ligands bind in nAChRs are possibly situated between the interfaces of heteromeric neuronal nAChRs, the principal faces of which are conferred by a non- $\alpha$  subunit (90). The neuronal non- $\alpha$  subunits do not contain the vicinal cysteine residues in their loop C, but this does not seem to affect the binding of galanthamine or cocaine, because the binding of these ligands to the AChBP is not affected by elimination of these cysteine residues (90).

### CONFORMATIONAL TRANSITIONS OF THE nAChR AND CHANNEL OPENING

Comparison of the crystal structures of the agonist-bound AChBPs with those of the ligand-free AChBP (apo-form), antagonist-bound AChBPs,  $\alpha$ -Btx-bound mouse nAChR  $\alpha 1$ -ECD, and the 4 Å EM structure of the *Torpedo*  $\alpha 1$ -ECD reveals that significant conformational changes occur in the nAChR-ECD on agonist binding (22, 29, 91). The most marked rearrangements occur in loop C, which swings as much as 11 Å between the two extreme positions observed in the complexes of the AChBP with  $\alpha$ -Ctx-ImI (antagonist) and epibatidine (agonist) (22) (Fig. 6). All the above structures are therefore classified into two categories with respect to C loop conformation, which is either “open” or “closed” (Fig. 6A) (22, 92). The first category includes the X-ray crystal structures of the ligand-free AChBP, antagonist-bound AChBPs,  $\alpha$ -Btx-bound  $\alpha 1$ -ECD, and the 4 Å EM structure of the *Torpedo* nAChR  $\alpha 1$ -ECD, representing the resting or desensitized state of nAChR-ECDs. The second category includes the structures of the agonist-bound AChBPs, which represent the activated state of the nAChR-ECDs. Furthermore, following agonist binding to the AChBP, rigid body movements of the  $\beta 1$ – $\beta 2$  loop and Cys-loop are also observed, with the loops moving upward, away from the bottom of the protein (91). Agonist binding in the intact nAChR could thus lead to the movement of the equivalent nAChR-ECD loops upward, away from the membrane plane.

These observations are consistent with the different orientation of the inner  $\beta$ -sheets in the  $\alpha$ -ECDs and those in the non- $\alpha$ -ECDs, as seen in the *Torpedo* nAChR 4 Å EM structure (28), the former being rotated  $\sim 10^\circ$  relative to the latter about an axis normal to the plane of the membrane. In this distorted conformation of the  $\alpha$  subunits, loop C projects away from the body of the  $\alpha$  subunits, in contrast to the situation in the agonist-bound AChBPs, where loop C is closer to loops A and B. Unwin suggested that, upon ACh binding, the distorted structural elements in  $\alpha$ -ECD move to their relaxed non- $\alpha$  positions, with loop C significantly twisting and rotating anticlockwise to allow coordination of the binding residues to ACh (28).

The conformational changes that occur in the nAChR  $\alpha$ -ECDs following agonist binding could be transmitted to the TMD, where the gate of the channel is located, through the  $\beta 10$  strand, which is covalently connected to the M1 helix of the TMD, and/or through the Cys-loop and  $\beta 1$ – $\beta 2$  loop, which

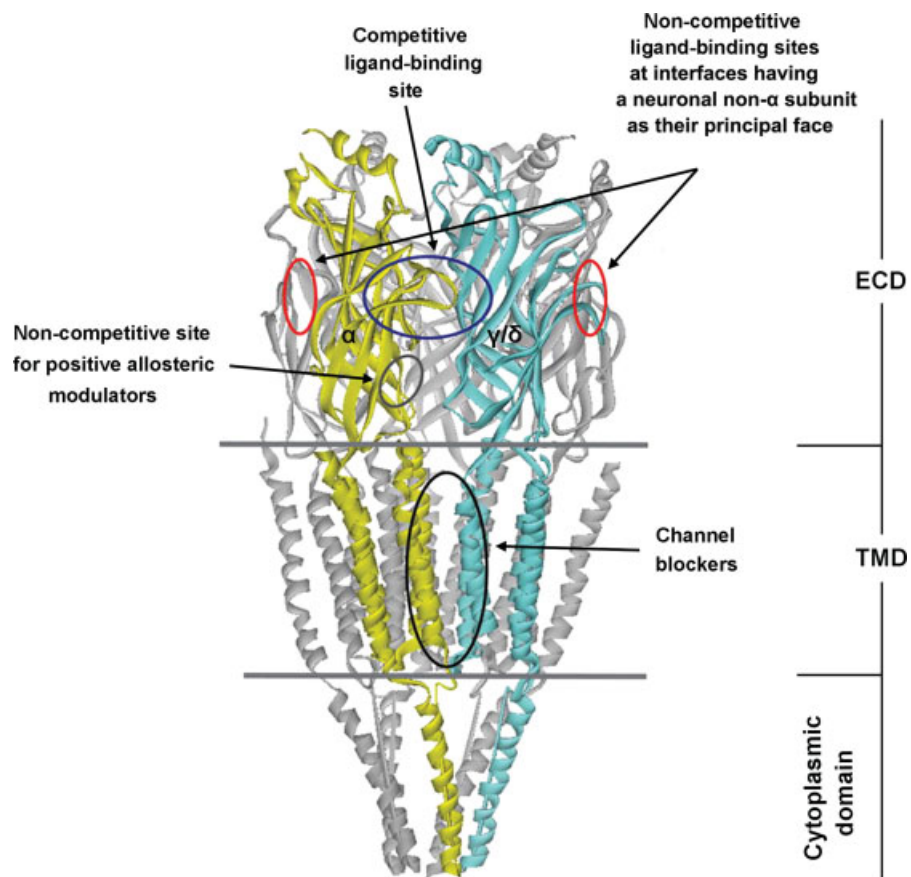


**Figure 5.** Schematic representation of the location of competitive and noncompetitive ligand-binding sites in nAChRs. The red ovals indicate the positions of noncompetitive (allosteric) ligand-binding sites on heteromeric neuronal nAChRs, in which a non- $\alpha$  neuronal subunit takes the place of the  $\gamma$  or  $\delta$  subunit in the Figure. Competitive ligand-binding sites (blue ovals) are also formed at the interfaces between some neuronal  $\alpha$  subunits (in homomeric  $\alpha 7$ ,  $\alpha 8$ , and  $\alpha 9$  nAChRs) and between several neuronal  $\alpha$  ( $\alpha 2-4$  or  $\alpha 6$ ) and  $\beta$  subunits ( $\beta 2$  or  $\beta 4$ ) in heteromeric neuronal nAChRs. Reproduced with permission from Hansen and Taylor, *J. Mol. Biol.*, 2007, 369, 895–901.

interact with amino acids in the M2-M3 loop of the TMD. More specifically, the Cys-loop interacts with amino acid residues near the N-terminus of M3 and the  $\beta 1-\beta 2$  loop interacts with residues near the C-terminus of M2 (Fig. 2C). Unwin proposed that the opening of the channel gate after agonist binding to the ECD could take place in two alternative ways (28): (a) both the displaced  $\beta 1-\beta 2$  loop and Cys-loop rotate back toward their relaxed non- $\alpha$  locations and no longer interact with residues of the M2-M3 segment, allowing movement of the M2-M3 loop because of the flexibility afforded by a conserved  $\alpha$ Gly residue at the end of M3, and thus allowing gating motions to occur; or (b) during the displacement of the  $\beta 1-\beta 2$  loop and Cys-loop, the interaction with the  $\beta 1-\beta 2$  loop is maintained and the movement of the loop drags the end of M2 away from the axis of the channel, breaking the interactions holding the M2 helices of the gate together, so that the channel opens.

Furthermore, the structure of the mouse  $\alpha 1$ -ECD revealed the existence of a hydration pocket inside the  $\beta$ -sandwich core, which

would be close to the TMD in the intact receptor (29). This contains a water molecule trapped between two buried hydrophilic residues (Thr52 and Ser126) and is connected to the outside through another water molecule to reach the surface residue Asn94 on loop A (Fig. 3C). This hydration pocket could therefore also transmit the conformational changes in the ECD, seen on agonist binding, to the TMD and lead to channel opening. Both hydrophilic residues (Thr52 and Ser126) are highly conserved in nAChRs, whereas the nonchannel homologous AChBP has bulky hydrophobic residues (Val/Leu and Phe) at these positions. Notably, mutations of Thr52 and Ser126 residues of the nAChR  $\alpha 1$  subunits to their hydrophobic counterparts in AChBP led to a significant reduction in ionic current flow through the cell membrane of transfected COS cells expressing these mutant nAChRs, confirming the importance of these residues for gating in the intact nAChR (29). This structural feature, which is unique to nAChRs, and does not exist in the nonchannel AChBP, could be a key element required for the nAChRs to function as LGICs.

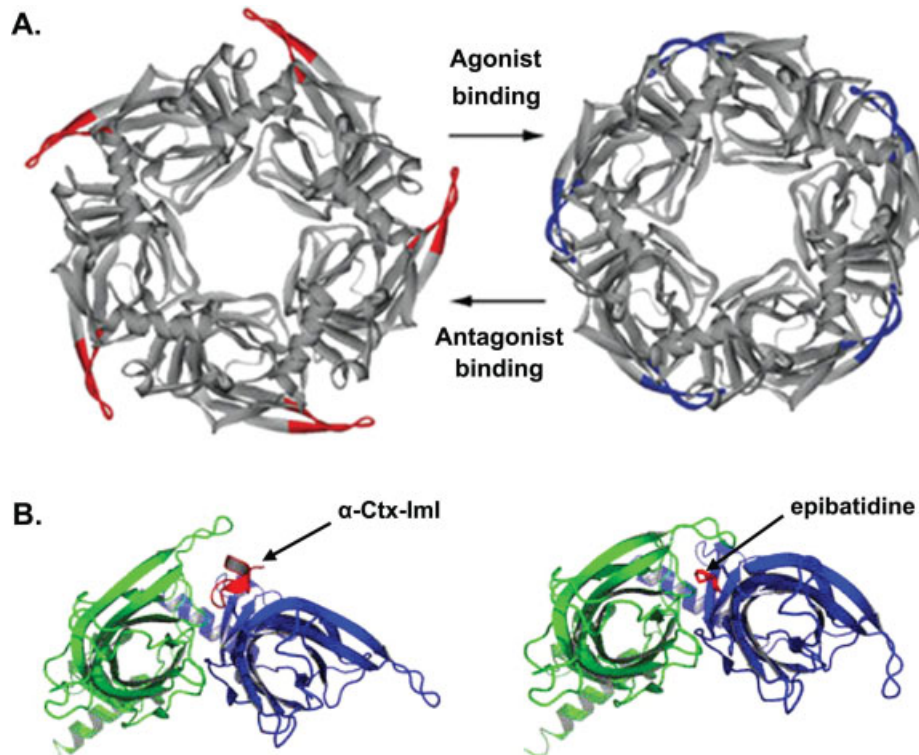


**Figure 6.** Conformational changes in loop C in AChBPs on competitive ligand-binding. Comparison of the orientation of loop C between two extreme positions, with  $\alpha$ -Ctx-Iml (antagonist) or epibatidine (agonist) bound to the A-AChBP. (A) Top view of the complexes, showing the “open” and “closed” configurations of loop C after binding of  $\alpha$ -Ctx-Iml (on the left; red loop C) or epibatidine (on the right; blue loop C), respectively, to A-AChBP. These complexes are used as models for showing the different orientation of loop C in AChBPs and nAChR-ECDs, upon binding of agonists or antagonists. (B) Detailed side-view of the complexes, showing the binding of  $\alpha$ -Ctx-Iml or epibatidine to one AChBP ligand-binding site. Loop C swings as much as 11 Å on going from one complex to the other. Reproduced with permission from Hansen et al., *EMBO J.*, 2005, 24, 3635–3646 and Duttre and Lewis, *Biochem. Pharmacol.*, 2006, 72, 661–670.

More recently (93), Auerbach and coworkers proposed a gating scenario for the muscle nAChR, using a method called rate equilibrium linear free energy analysis (REFER analysis) (94). This method compares changes in the opening rate to changes in the equilibrium between closed and open states, when a specific amino acid residue is mutated to several types; it then estimates  $\varphi$ -value, a fraction between 0 and 1, which quantifies the extent to which a local site in the protein has progressed in the gating reaction at the transition state (TS) between the stable closed and open states. Higher  $\varphi$ -values indicate earlier, lower  $\varphi$ -values indicate later, and equivalent  $\varphi$ -values indicate synchronized gating motions. REFER analyses of hundreds of residues indicated that the nAChR is organized into several domains (blocks) within which  $\varphi$ -values are indistinguishable (93, 95). Moreover, there is a spatial gradient in block  $\varphi$ -values, which approximately follows the long axis of the muscle nAChR, ranging from  $\sim 1$  in the vicinity of the transmitter binding site (TBS) to  $\sim 0$  in the middle of the TMD (93, 96), during channel opening. This pattern suggests that the framework for

the gating mechanism is that of a Brownian conformational wave, connecting structural changes that regulate transmitter affinity with those that regulate conductance (97).

Regarding each muscle nAChR  $\alpha$  subunit, the proposed gating scenario from such studies is as follows (93): Upon agonist binding, loops A, B, C of the TBS and three residues (Ile260, Pro265, and Ser268) of the C-terminus of the pore-lining  $\alpha$ M2-helix, referred to as M2-cap (residues  $\alpha$ 260– $\alpha$ 270), move rapidly and at the same time ( $\varphi = 0.94$ ) announcing the exit of the nAChR from the stable closed state and its entry into the TS ensemble. The motions of the TBS and the M2-cap trigger those in the adjacent  $\beta$ 1– $\beta$ 2 loop and the Cys-loop, which together with four residues of the M2-cap (Val261, Glu262, Ile264, and Thr267) constitute the second block ( $\varphi = 0.78$ ) (98). These motions provoke the movement of a third block, involving residues in the M2–M3 linker (98) and most of M2 (also involving residues Leu263, Ser266, Ser269, and Ala270 of the M2-cap) ( $\varphi = 0.64$ ) (95), which propagate to the fourth block consisting of residues in the middle of M2 and beyond,

and in M4 ( $\varphi = 0.54$ ) (98). Eventually, these motions destabilize the residues Leu251 and Thr254 of M2 (residues 9' and 12' of  $\alpha$ M2, respectively) near the equator, which are believed to be major components of the gate of the channel (39, 48) and residues of M3 ( $\varphi = 0.31$ ) (93). The movement of the M2 equator reflects the entry into the open structural ensemble.

It should be noted that investigations involving REFER analysis have also been made for various structural elements of the non- $\alpha$  subunits, as well. Briefly, it has been shown that  $\epsilon$ M4 ( $\varphi = 0.33$ ) and  $\beta$ M4 ( $\varphi = 0.17$ ) move as rigid bodies after the rigid body motion of both  $\alpha$ M4-helices ( $\varphi = 0.54$ ), whereas  $\epsilon$ M4 does not move at all (99).  $\varphi$ -values have also been estimated for  $\epsilon$ M2–M3 and  $\beta$ M2–M3 linkers (0.57 and 0.43, respectively) and for  $\delta$ M2 (100). In the case of  $\delta$ M2, it seems that its upper half moves earlier than the lower half, because the former has  $\varphi = 0.32$  and the latter has  $\varphi = 0$ , with the lower half of  $\delta$ M2 being one of the domains that move lastly in the overall gating process. All these determined  $\varphi$ -values provide an almost complete map of  $\varphi$ -values for the long axis of the muscle nAChR, revealing the dynamics of the nAChR gating mechanism (93, 95).

What is surprising with this gating scenario is that  $\alpha$ M2-cap seems to move at the same time with the TBS and earlier than the M2–M3 linker and the adjacent  $\beta$ 1– $\beta$ 2 loop and Cys-loop, in contrast with what Unwin had previously suggested (28). In the *Torpedo* nAChR structure, there seems to be no direct connection between loops A, B, and C of the TBS with  $\alpha$ M2-cap. However, this structure represents the unliganded nAChR. It is possible that upon agonist binding, TBS and  $\alpha$ M2-cap move closer than they are in the closed *Torpedo* nAChR structural model and in fact may make direct interactions. Another possibility, also proposed by Auerbach and coworkers (93), is that there may be physical connections between TBS and  $\alpha$ M2-cap (e.g., electrostatic interactions or interactions via water molecules), which cannot be seen in the electron density maps. Such a physical connection might be the hydration cavity revealed in the crystal structure of mouse nAChR  $\alpha$ 1-ECD (29), which extended from the lower part of  $\alpha$ 1-ECD up to loop A of the TBS, as discussed earlier. Apparently, for this scenario to be confirmed, high resolution structures of both closed and open structural ensembles of the nAChR are needed. In summary, Auerbach and coworkers' findings suggest that after agonist binding, the nAChR moves through a number of intermediate states, the so called "conformational wave," before channel opening.

A latest work (101) showed that the properties of the intermediate conformations of nAChR residues during gating, referred to as "flip," can be indeed detected and measured. In addition, the results of this study reinterpret what was until recently known regarding the difference between full and partial agonists. In principle, when a partial agonist binds to a receptor, it cannot produce the large response, evident in the case of a fully efficacious agonist. It has been believed since 1950 that this is because a full agonist has a higher affinity for the open

state than the closed state, and therefore its binding shifts the equilibrium toward the open state. However, Lape et al. (101) showed, using full and partial agonists for GlyR (glycine and taurine, respectively) and nAChR (ACh and tetramethylammonium, respectively), that what makes an agonist partial is a low affinity for the intermediate "flipped" state, relative to the resting state, rather than low affinity for the open state, relative to the resting state, as previously believed. Therefore, the effectiveness of an agonist depends on its relative affinity for resting and "flipped" conformations. Once the channel has reached the "flipped" intermediate state, or the intermediate preopen state, channel opening occurs with the same rate, regardless of which agonist (full or partial) is bound. In other words, a partial agonist when bound to a receptor produces lower responses of the channel than a full agonist, because the rate of transition of the channel from its resting state to the flipped state (flipping equilibrium constant) is lower than in the case of binding of a full agonist. The results of this study are consistent with a previous study, which had shown that the differences between the response of nAChR to various nicotinic agonists, detected by measurements of  $\varphi$ -values, lie early in the activation process close to the TBS (96).

## CONCLUSIONS AND FUTURE PERSPECTIVES

The availability over the last few years of high-resolution X-ray crystal structures for AChBPs, structural analogues of nAChR-ECDs, in their ligand-free and ligand-bound forms, and for the  $\alpha$ -Btx-bound mouse nAChR  $\alpha$ 1-ECD and two prokaryotic LGICs (ELIC and GLIC), together with the 4 Å resolution EM structure of the *Torpedo* nAChR, have greatly increased our knowledge regarding nAChR structure and function. These breakthrough studies revealed atomic details for the binding of both competitive and noncompetitive ligands to nAChRs, provided important insights into the gating mechanism of nAChRs, and were used to develop the "quaternary state model" for the transition between the different states of the nAChR (102, 103). According to this model, the nAChR functions as an allosteric protein, transmitting the conformational changes induced in its ECD, upon agonist binding, to the topographically distinct gate, leading to channel opening.

The data on the ECD and TMD of nAChR obtained by these studies have been used to create 3D molecular models for various nAChR subtypes [e.g., (102–106)], which could serve as templates for structure-guided drug design to treat various neurological conditions associated with the orthosteric or allosteric nAChR ligand-binding sites, such as Alzheimer's and Parkinson's diseases, schizophrenia, pain, depression, and nicotine addiction.

However, the main difficulty in drug design is that at least 12 genes code for the neuronal nAChR subunits, and their gene products ( $9\alpha$  and  $3\beta$  subunits) assemble in various combinations, forming a broad diversity of pentamers with distinct pharmacological properties. Clearly, to treat pathological conditions

involving one or another of the neuronal subtypes, a subtype-specific drug design approach is needed. The large majority of known nAChR ligands are not subtype-specific (107). For example, varenicline, a nicotinic compound, recently approved as a drug against smoking addiction, is a full agonist of  $\alpha 7$ , a potent partial agonist of  $\alpha 4\beta 2$ , and has lower efficacy and potency for  $\alpha 3\beta 4$  (108). Accordingly, the identification of subtype-selective compounds that make use of the beneficial effects of nicotine, while eliminating or decreasing its adverse effects, continues to be a challenging area of research. Antagonists might help to distinguish between subtypes: for instance, MLA inhibits  $\alpha 7$ , but not the heteromeric receptors, and  $\alpha$ -Ctx-MII selectively tags  $\alpha 3$ - and  $\alpha 6$ -containing nAChRs, whereas  $\alpha$ -Btx blocks the  $\alpha 7$ ,  $\alpha 8$ ,  $\alpha 9$ , and  $\alpha 10$  as well as the muscle-type nAChRs (109).

The subunit interfaces of neuronal heteromeric nAChRs with a non- $\alpha$  subunit on their principal faces probably host noncompetitive ligand-binding sites and may prove useful in developing subtype-selective compounds for treating several pathological conditions and for studying receptor subtype assembly and localization (90). Non- $\alpha$  neuronal nAChR subunits exhibit a higher degree of sequence variation in loop C than the  $\alpha$  subunits, which contribute to the formation of competitive ligand-binding sites. They therefore represent potential targets for treating various neuronal nAChR-related diseases and for developing subtype-selective drugs. A novel group of positive allosteric modulators potentiating  $\alpha 7$  nAChRs includes the polypeptide lynx1 (110), which is the endogenous brain structural homologue of  $\alpha$ -Btx, and synthetic compounds enhancing cognition properties in humans [e.g., compound 6 (111) or NS 1738 (112)]. Negative allosteric modulators of nAChRs are well known and include histrionicotoxin, PCP, and MK-801 (113).

Regarding human muscle nAChRs, the accumulated knowledge on nAChR structure may help in understanding how various reported mutations cause the slow- or fast-channel congenital myasthenic syndromes [reviewed in (91)] and in the development of structure-guided therapeutic strategies. The elucidation of the structure of the MIR epitope in atomic detail (29) could also facilitate the development of structure-guided therapeutic treatments for MG. Given the availability of high-resolution X-ray crystal structures for several Fab domains of monoclonal anti-MIR antibodies, such as Fab198 (114) or Fab192 (115), which inhibit the pathogenic activity of intact anti-nAChR antibodies (14, 116), useful modeling and docking studies can be performed. A recent example is the docking of Fab198 to the MIR epitope of the *Torpedo*  $\alpha$ -ECD (117), which revealed the antigen-antibody interactions and helped propose the design of mutant antibody fragments with enhanced binding affinity for the MIR epitope. Such studies can now be validated and/or utilized using the mouse  $\alpha 1$  MIR structure in similar docking approaches.

However, despite the significant progress in understanding nAChR structure, the high-resolution structure of a complete nAChR and/or of a complete ligand-binding site is still lacking.

As crystallization of the intact nAChR is a difficult task because of its large hydrophobic TMD, efforts to crystallize only its ECD, as in the case of the mouse  $\alpha 1$ -ECD (29), seem a more realistic approach. Toward this goal, we have expressed various human nAChR-ECDs in bacterial or eukaryotic expression systems and performed several mutations to improve their solubility and facilitate their crystallization. For example, the replacement of the nAChR Cys-loop by the corresponding and more hydrophilic loop region from the L-AChBP greatly increased the solubility of the expressed neuronal  $\alpha 7$ -ECD (83) and the muscle  $\gamma$ -ECD (118). Additionally, based on a constructed 3D homology model for the human  $\alpha 7$ -ECD, using the EM structure of the *Torpedo* nAChR and the crystal structure of L-AChBP as templates, we inserted several site-directed mutations to the AChBP Cys-loop-containing  $\alpha 7$ -ECD (83), which further enhanced its solubility and ligand-binding properties and led to its expression in what is probably a pentameric form, rendering it a promising novel mutant for crystallization (119).

Overall, the detailed information on the nAChR structure-function relationship that has been obtained during the last few years forms the basis for our understanding of key elements in neurotransmission and of structural differences between the allosteric states of nAChR, and for the design of nAChR subtype-specific ligands as safe and potent drugs for a multitude of important and devastating neuropsychiatric and neurodegenerative diseases, for stopping smoking, and for treating muscle diseases. The anticipated elucidation of the structure of intact human nAChRs, or at least of their intact ligand-binding domains, would dramatically facilitate the achievement of these major targets.

## ACKNOWLEDGEMENTS

The original work in the authors' laboratories described in this review was supported by a PENED grant (co-financed 80% by the EU-European Social Fund and 20% by the Greek Ministry of Development-GSRT) and by the EC FP7 project Neuro-Cypres (no. 202088).

## REFERENCES

- Lester, H. A., Dibas, M. I., Dahan, D. S., Leite, J. F., and Dougherty, D. A. (2004) Cys-loop receptors: new twists and turns. *Trends Neurosci.* **27**, 329–336.
- Kalamida, D., Poulas, K., Avramopoulou, V., Fostieri, E., Lagoumintzis, G., Lazaridis, K., Sideri, A., Zouridakis, M., and Tzartos, S. J. (2007) Muscle and neuronal nicotinic acetylcholine receptors: structure, function and pathogenicity. *FEBS J.* **274**, 3799–3845.
- Noda, M., Takahashi, H., Tanabe, T., Toyosato, M., Furutani, Y., Hirose, T., Asai, M., Inayama, S., Miyata, T., and Numa, S. (1982) Primary structure of  $\alpha$ -subunit precursor of *Torpedo californica* acetylcholine receptor deduced from cDNA sequence. *Nature* **299**, 793–797.
- Gotti, C. and Clementi, F. (2004) Neuronal nicotinic receptors: from structure to pathology. *Prog. Neurobiol.* **74**, 363–396.
- Blount, P. and Merlie, J. P. (1989) Molecular basis of the two nonequivalent ligand binding sites of the muscle nicotinic acetylcholine receptor. *Neuron* **33**, 349–357.
- Le Novere, N., Zoli, M., and Changeux, J. P. (1996) Neuronal nicotinic receptor  $\alpha 6$  subunit mRNA is selectively concentrated in

- catecholaminergic nuclei of the rat brain. *Eur. J. Neurosci.* **8**, 2428–2439.
7. Gaimarri, A., Moretti, M., Riganti, L., Zanardi, A., Clementi, F., and Gotti, C. (2007) Regulation of neuronal nicotinic receptor traffic and expression. *Brain Res. Rev.* **55**, 134–143.
  8. Paterson, D. and Nordberg, A. (2000) Neuronal nicotinic receptors in the human brain. *Prog. Neurobiol.* **61**, 75–111.
  9. Gahring, L. C. and Rogers, S. W. (2005) Neuronal nicotinic acetylcholine receptor expression and function on nonneuronal cells. *AAPS J.* **7**, E885–E894.
  10. Raymond-Delpech, V., Matsuda, K., Sattelle, B. M., Rauh, J. J., and Sattelle, D. B. (2005) Ion channels: molecular targets of neuroactive insecticides. *Invert Neurosci.* **5**, 119–133.
  11. Fucile, S. (2004) Ca<sup>2+</sup> permeability of nicotinic acetylcholine receptors. *Cell Calcium* **35**, 1–8.
  12. Beroukhim, R. and Unwin, N. (1995) Three-dimensional location of the main immunogenic region of the acetylcholine receptor. *Neuron* **15**, 323–331.
  13. Tzartos, S. J., Barkas, T., Cung, M. T., Mamalaki, A., Marraud, M., Orlewski, P., Papanastasiou, D., Sakarellos, C., Sakarellos-Daitsiotis, M., Tsantili, P., and Tsikaris, V. (1998) Anatomy of the antigenic structure of a large membrane autoantigen, the muscle-type nicotinic acetylcholine receptor. *Immunol. Rev.* **163**, 89–120.
  14. Papanastasiou, D., Mamalaki, A., Eliopoulos, E., Poulas, K., Liolitas, C., and Tzartos, S. J. (1999) Construction and characterization of a humanized single chain Fv antibody fragment against the main immunogenic region of the acetylcholine receptor. *J. Neuroimmunol.* **94**, 182–195.
  15. Engel, A. G., Ohno, K., and Sine, S. M. (1998) Congenital myasthenic syndromes: experiments of nature. *J. Physiol. (Paris)* **92**, 113–117.
  16. Nichols, P., Croxen, R., Vincent, A., Rutter, R., Hutchinson, M., Newsom-Davis, J., and Beeson, D. (1999) Mutation of the acetylcholine receptor epsilon-subunit promoter in congenital myasthenic syndrome. *Ann. Neurol.* **45**, 439–443.
  17. Steinlein, O. K., Mulley, J. C., Propping, P., Wallace, R. H., Phillips, H. A., Sutherland, G. R., Scheffer, I. E., and Berkovic, S. F. (1995) A missense mutation in the neuronal nicotinic acetylcholine receptor  $\alpha$  4 subunit is associated with autosomal dominant nocturnal frontal lobe epilepsy. *Nat. Genet.* **11**, 201–203.
  18. Kuryatov, A., Gerzanich, V., Nelson, M., Olale, F., and Lindstrom, J. (1997) Mutation causing autosomal dominant nocturnal frontal lobe epilepsy alters Ca<sup>2+</sup> permeability, conductance, and gating of human  $\alpha$ 4 $\beta$ 2 nicotinic acetylcholine receptors. *J. Neurosci.* **17**, 9035–9047.
  19. Brody, A. L. (2006) Functional brain imaging of tobacco use and dependence. *J. Psychiatr. Res.* **40**, 404–418.
  20. Brejc, K., van Dijk, W. J., Klaassen, R. V., Schuurmans, M., van Der Oost, J., Smit, A. B., and Sixma, T. K. (2001) Crystal structure of an ACh-binding protein reveals the ligand-binding domain of nicotinic receptors. *Nature* **411**, 269–276.
  21. Celie, P. H., van Rossum-Fikkert, S. E., van Dijk, W. J., Brejc, K., Smit, A. B., and Sixma, T. K. (2004) Nicotine and carbamylcholine binding to nicotinic acetylcholine receptors as studied in AChBP crystal structures. *Neuron* **41**, 907–914.
  22. Hansen, S. B., Sulzenbacher, G., Huxford, T., Marchot, P., Taylor, P., and Bourne, Y. (2005) Structures of *Aplysia* AChBP complexes with nicotinic agonists and antagonists reveal distinctive binding interfaces and conformations. *EMBO J.* **24**, 3635–3646.
  23. Celie, P. H., Kasheverov, I. E., Mordvintsev, D. Y., Hogg, R. C., van Nierop, P., van Elk, R., van Rossum-Fikkert, S. E., Zhmak, M. N., Bertrand, D., Tsetlin, V., Sixma, T. K., and Smit, A. B. (2005) Crystal structure of nicotinic acetylcholine receptor homolog AChBP in complex with an  $\alpha$ -conotoxin PnIA variant. *Nat. Struct. Mol. Biol.* **12**, 582–588.
  24. Celie, P. H., Klaassen, R. V., van Rossum-Fikkert, S. E., van Elk, R., van Nierop, P., Smit, A. B., and Sixma, T. K. (2005) Crystal structure of acetylcholine-binding protein from *Bulinus truncatus* reveals the conserved structural scaffold and sites of variation in nicotinic acetylcholine receptors. *J. Biol. Chem.* **280**, 26457–26466.
  25. Bourne, Y., Talley, T. T., Hansen, S. B., Taylor, P., and Marchot, P. (2005) Crystal structure of a CbtX-AChBP complex reveals essential interactions between snake  $\alpha$ -neurotoxins and nicotinic receptors. *EMBO J.* **24**, 1512–1522.
  26. Ulens, C., Hogg, R. C., Celie, P. H., Bertrand, D., Tsetlin, V., Smit, A. B., and Sixma, T. K. (2006) Structural determinants of selective  $\alpha$ -conotoxin binding to a nicotinic acetylcholine receptor homolog AChBP. *Proc. Natl. Acad. Sci. USA* **103**, 3615–3620.
  27. Dutertre, S., Ulens, C., Buttner, R., Fish, A., van Elk, R., Kendel, Y., Hopping, G., Alewood, P. F., Schroeder, C., Nicke, A., Smit, A. B., Sixma, T. K., and Lewis, R. J. (2007) AChBP-targeted  $\alpha$ -conotoxin correlates distinct binding orientations with nAChR subtype selectivity. *EMBO J.* **26**, 3858–3867.
  28. Unwin, N. (2005) Refined structure of the nicotinic acetylcholine receptor at 4 Å resolution. *J. Mol. Biol.* **346**, 967–989.
  29. Dellisanti, C. D., Yao, Y., Stroud, J. C., Wang, Z. Z., and Chen, L. (2007) Crystal structure of the extracellular domain of nAChR  $\alpha$ 1 bound to  $\alpha$ -bungarotoxin at 1.94 Å resolution. *Nat. Neurosci.* **10**, 953–962.
  30. Hilf, R. J. and Dutzler, R. (2008) X-ray structure of a prokaryotic pentameric ligand-gated ion channel. *Nature* **452**, 375–379.
  31. Hilf, R. J. and Dutzler, R. Structure of a potentially open state of a proton-activated pentameric ligand-gated ion channel. *Nature*, in press; doi:10.1038/nature07461.
  32. Bocquet, N., Nury, H., Baaden, M., Le Poupon, C., Changeux, J. P., Delarue, M., and Corringer, P. J. X-ray structure of a pentameric ligand-gated ion channel in an apparently open conformation. *Nature*, in press; doi: 10.1038/nature07462.
  33. Unwin, N. (1993) Nicotinic acetylcholine receptor at 9 Å resolution. *J. Mol. Biol.* **229**, 1101–1124.
  34. Unwin, N. (1995) Acetylcholine receptor channel imaged in the open state. *Nature* **373**, 37–43.
  35. Smit, A. B., Syed, N. I., Schaap, D., van Minnen, J., Klumperman, J., Kits, K. S., Lodder, H., van der Schors, R. C., van Elk, R., Sorgedrager, B., Brejc, K., Sixma, T. K., and Geraerts, W. P. (2001) A glia-derived acetylcholine-binding protein that modulates synaptic transmission. *Nature* **411**, 261–268.
  36. Bouzat, C., Gumilar, F., Spitzmaul, G., Wang, H. L., Rayes, D., Hansen, S. B., Taylor, P., and Sine, S. M. (2004) Coupling of agonist binding to channel gating in an ACh-binding protein linked to an ion channel. *Nature* **430**, 896–900.
  37. Sixma, T. K. and Smit, A. B. (2003) Acetylcholine binding protein (AChBP): a secreted glial protein that provides a high-resolution model for the extracellular domain of pentameric ligand-gated ion channels. *Annu. Rev. Biophys. Biomol. Struct.* **32**, 311–334.
  38. Miyazawa, A., Fujiyoshi, Y., Stowell, M., and Unwin, N. (1999) Nicotinic acetylcholine receptor at 4.6 Å resolution: transverse tunnels in the channel wall. *J. Mol. Biol.* **288**, 765–786.
  39. Miyazawa, A., Fujiyoshi, Y., and Unwin, N. (2003) Structure and gating mechanism of the acetylcholine receptor pore. *Nature* **423**, 949–955.
  40. Galzi, J. L., Revah, F., Bouet, F., Menez, A., Goeldner, M., Hirth, C., and Changeux, J. P. (1991) Allosteric transitions of the acetylcholine receptor probed at the amino acid level with a photolabile cholinergic ligand. *Proc. Natl. Acad. Sci. USA* **88**, 5051–5055.
  41. Arias, H. R. (2000) Localization of agonist and competitive antagonist binding sites on nicotinic acetylcholine receptors. *Neurochem. Int.* **36**, 595–645.
  42. Corringer, P. J., Le Novère, N., and Changeux, J. P. (2000) Nicotinic receptors at the amino acid level. *Annu. Rev. Pharmacol. Toxicol.* **40**, 431–458.

43. Tzartos, S. J., Kokla, A., Walgrave, S. L., and Conti-Tronconi, B. M. (1988) Localization of the main immunogenic region of human muscle acetylcholine receptor to residues 67–76 of the  $\alpha$  subunit. *Proc. Natl. Acad. Sci. USA* **85**, 2899–2903.
44. Papadouli, I., Sakarellos, C., and Tzartos, S. J. (1993) High-resolution epitope mapping and fine antigenic characterization of the main immunogenic region of the acetylcholine receptor. Improving the binding activity of synthetic analogues of the region. *Eur. J. Biochem.* **211**, 227–234.
45. Tzartos, S. J., Tsantili, P., Papanastasiou, D., and Mamalaki, A. (1998) Construction of single-chain Fv fragments of anti-MIR monoclonal antibodies. *Ann. N. Y. Acad. Sci.* **841**, 475–477.
46. Bocquet, N., Prado de Carvalho, L., Cartaud, J., Neyton, J., Le Poupon, C., Taly, A., Grutter, T., Changeux, J. P., and Corringer, P. J. (2007) A prokaryotic proton-gated ion channel from the nicotinic acetylcholine receptor family. *Nature* **445**, 116–119.
47. Zouridakis, M., Kostelidou, K., Sotiriadis, A., Stergiou, C., Eliopoulos, E., Poulas, K., and Tzartos, S. J. (2007) Circular dichroism studies of extracellular domains of human nicotinic acetylcholine receptors provide an insight into their structure. *Int. J. Biol. Macromol.* **41**, 423–429.
48. Unwin, N. (2003) Structure and action of the nicotinic acetylcholine receptor explored by electron microscopy. *FEBS Lett.* **555**, 91–95.
49. Kottwitz, D., Kukhtina, V., Dergousova, N., Alexeev, T., Utkin, Y., Tsetlin, V., and Hucho, F. (2004) Intracellular domains of the  $\delta$ -subunits of *Torpedo* and rat acetylcholine receptors—expression, purification, and characterization. *Protein Expr. Purif.* **38**, 237–247.
50. Kukhtina, V., Kottwitz, D., Strauss, H., Heise, B., Chebotareva, N., Tsetlin, V., and Hucho, F. (2006) Intracellular domain of nicotinic acetylcholine receptor: the importance of being unfolded. *J. Neurochem.* **97**, (Suppl 1), 63–67.
51. Dyson, H. J. and Wright, P. E. (2005) Intrinsically unstructured proteins and their functions. *Nat. Rev. Mol. Cell. Biol.* **6**, 197–208.
52. Yu, X. M. and Hall, Z. W. (1994) The role of the cytoplasmic domains of individual subunits of the acetylcholine receptor in 43 kDa protein-induced clustering in COS cells. *J. Neurosci.* **14**, 785–795.
53. Valor, L. M., Mulet, J., Sala, F., Sala, S., Ballesta, J. J., and Criado, M. (2002) Role of the large cytoplasmic loop of the  $\alpha 7$  neuronal nicotinic acetylcholine receptor subunit in receptor expression and function. *Biochemistry* **41**, 7931–7938.
54. Kuo, Y. P., Xu, L., Eaton, J. B., Zhao, L., Wu, J., and Lukas, R. J. (2005) Roles for nicotinic acetylcholine receptor subunit large cytoplasmic loop sequences in receptor expression and function. *J. Pharmacol. Exp. Ther.* **314**, 455–466.
55. Castelan, F., Mulet, J., Aldea, M., Sala, S., Sala, F., and Criado, M. (2007) Cytoplasmic regions adjacent to the M3 and M4 transmembrane segments influence expression and function of  $\alpha 7$  nicotinic acetylcholine receptors. A study with single amino acid mutants. *J. Neurochem.* **100**, 406–415.
56. Williams, B. M., Temburni, M. K., Levey, M. S., Bertrand, S., Bertrand, D., and Jacob, M. H. (1998) The long internal loop of the  $\alpha 3$  subunit targets nAChRs to subdomains within individual synapses on neurons in vivo. *Nat. Neurosci.* **1**, 557–562.
57. Williams, B. M., Temburni, M. K., Bertrand, S., Bertrand, D., and Jacob, M. H. (1999) The long cytoplasmic loop of the  $\alpha 3$  subunit targets specific nAChR subtypes to synapses on neurons in vivo. *Ann. N. Y. Acad. Sci.* **868**, 640–644.
58. Temburni, M. K., Blitzblau, R. C., and Jacob, M. H. (2000) Receptor targeting and heterogeneity at interneuronal nicotinic cholinergic synapses in vivo. *J. Physiol.* **525** (Part 1), 21–29.
59. Keller, S. H., Lindstrom, J., Ellisman, M., and Taylor, P. (2001) Adjacent basic amino acid residues recognized by the COP I complex and ubiquitination govern endoplasmic reticulum to cell surface trafficking of the nicotinic acetylcholine receptor  $\alpha$ -subunit. *J. Biol. Chem.* **276**, 18384–18391.
60. Ren, X. Q., Cheng, S. B., Treuil, M. W., Mukherjee, J., Rao, J., Braunevel, K. H., Lindstrom, J. M., and Anand, R. (2005) Structural determinants of  $\alpha 4\beta 2$  nicotinic acetylcholine receptor trafficking. *J. Neurosci.* **25**, 6676–6686.
61. Xu, J., Zhu, Y., and Heinemann, S. F. (2006) Identification of sequence motifs that target neuronal nicotinic receptors to dendrites and axons. *J. Neurosci.* **26**, 9780–9793.
62. Bencherif, M. and Lukas, R. J. (1993) Cytochalasin modulation of nicotinic cholinergic receptor expression and muscarinic receptor function in human TE671/RD cells: a possible functional role of the cytoskeleton. *J. Neurochem.* **61**, 852–864.
63. Maimone, M. M. and Enigk, R. E. (1999) The intracellular domain of the nicotinic acetylcholine receptor  $\alpha$  subunit mediates its co-clustering with rapsyn. *Mol. Cell Neurosci.* **14**, 340–354.
64. Feng, G., Steinbach, J. H., and Sanes, J. R. (1998) Rapsyn clusters neuronal acetylcholine receptors but is inessential for formation of an interneuronal cholinergic synapse. *J. Neurosci.* **18**, 4166–4176.
65. Shoop, R. D., Yamada, N., and Berg, D. K. (2000) Cytoskeletal links of neuronal acetylcholine receptors containing  $\alpha 7$  subunits. *J. Neurosci.* **20**, 4021–4029.
66. Bruneau, E. and Akaaboune, M. (2007) The dynamics of the rapsyn scaffolding protein at individual acetylcholine receptor clusters. *J. Biol. Chem.* **282**, 9932–9940.
67. Pacheco, M. A., Pastoor, T. E., and Wecker, L. (2003) Phosphorylation of the  $\alpha 4$  subunit of human  $\alpha 4\beta 2$  nicotinic receptors: role of cAMP-dependent protein kinase (PKA) and protein kinase C (PKC). *Brain Res. Mol. Brain Res.* **114**, 65–72.
68. Wiesner, A. and Fuhrer, C. (2006) Regulation of nicotinic acetylcholine receptors by tyrosine kinases in the peripheral and central nervous system: same players, different roles. *Cell Mol. Life Sci.* **63**, 2818–2828.
69. Haganir, R. L., Delcour, A. H., Greengard, P., and Hess, G. P. (1986) Phosphorylation of the nicotinic acetylcholine receptor regulates its rate of desensitization. *Nature* **321**, 774–776.
70. Fenster, C. P., Beckman, M. L., Parker, J. C., Sheffield, E. B., Whitworth, T. L., Quick, M. W., and Lester, R. A. (1999) Regulation of  $\alpha 4\beta 2$  nicotinic receptor desensitization by calcium and protein kinase C. *Mol. Pharmacol.* **55**, 432–443.
71. Wang, K., Hackett, J. T., Cox, M. E., Van Hoek, M., Lindstrom, J. M., and Parsons, S. J. (2004) Regulation of the neuronal nicotinic acetylcholine receptor by SRC family tyrosine kinases. *J. Biol. Chem.* **279**, 8779–8786.
72. Cho, C. H., Song, W., Leitzell, K., Teo, E., Meleth, A. D., Quick, M. W., and Lester, R. A. (2005) Rapid upregulation of  $\alpha 7$  nicotinic acetylcholine receptors by tyrosine dephosphorylation. *J. Neurosci.* **25**, 3712–3723.
73. Colledge, M. and Froehner, S. C. (1997) Tyrosine phosphorylation of nicotinic acetylcholine receptor mediates Grb2 binding. *J. Neurosci.* **17**, 5038–5045.
74. Huang, K. and El-Husseini, A. (2005) Modulation of neuronal protein trafficking and function by palmitoylation. *Curr. Opin. Neurobiol.* **15**, 527–535.
75. Drisdell, R. C., Alexander, J. K., Sayeed, A., and Green, W. N. (2006) Assays of protein palmitoylation. *Methods* **40**, 127–134.
76. Drisdell, R. C., Manzana, E., and Green, W. N. (2004) The role of palmitoylation in functional expression of nicotinic  $\alpha 7$  receptors. *J. Neurosci.* **24**, 10502–10510.
77. Grutter, T. and Changeux, J. P. (2001) Nicotinic receptors in wonderland. *Trends Biochem. Sci.* **26**, 459–463.
78. Neumann, D., Barchan, D., Fridkin, M., and Fuchs, S. (1986) Analysis of ligand binding to the synthetic dodecapeptide 185–196 of the acetylcholine receptor  $\alpha$  subunit. *Proc. Natl. Acad. Sci. USA* **83**, 9250–9253.

79. Tzartos, S. J. and Remoundos, M. S. (1990) Fine localization of the major  $\alpha$ -bungarotoxin binding site to residues  $\alpha$  189–195 of the *Torpedo* acetylcholine receptor. Residues 189, 190, and 195 are indispensable for binding. *J. Biol. Chem.* **265**, 21462–21467.
80. Moise, L., Piserchio, A., Basus, V. J., and Hawrot, E. (2002) NMR structural analysis of  $\alpha$ -bungarotoxin and its complex with the principal  $\alpha$ -neurotoxin-binding sequence on the  $\alpha$  7 subunit of a neuronal nicotinic acetylcholine receptor. *J. Biol. Chem.* **277**, 12406–12417.
81. Marinou, M. and Tzartos, S. J. (2003) Identification of regions involved in the binding of  $\alpha$ -bungarotoxin to the human  $\alpha$ 7 neuronal nicotinic acetylcholine receptor using synthetic peptides. *Biochem. J.* **372** (Part 2), 543–554.
82. Psaridi-Linardaki, L., Mamalaki, A., Remoundos, M., and Tzartos, S. J. (2002) Expression of soluble ligand- and antibody-binding extracellular domain of human muscle acetylcholine receptor  $\alpha$  subunit in yeast *Pichia pastoris*. Role of glycosylation in  $\alpha$ -bungarotoxin binding. *J. Biol. Chem.* **277**, 26980–26986.
83. Avramopoulou, V., Mamalaki, A., and Tzartos, S. J. (2004) Soluble, oligomeric, and ligand-binding extracellular domain of the human  $\alpha$ 7 acetylcholine receptor expressed in yeast: replacement of the hydrophobic cysteine loop by the hydrophilic loop of the ACh-binding protein enhances protein solubility. *J. Biol. Chem.* **279**, 38287–38293.
84. Pereira, E. F., Hilmas, C., Santos, M. D., Alkondon, M., Maelicke, A., and Albuquerque, E. X. (2002) Unconventional ligands and modulators of nicotinic receptors. *J. Neurobiol.* **53**, 479–500.
85. Hogg, R. C., Buisson, B., and Bertrand, D. (2005) Allosteric modulation of ligand-gated ion channels. *Biochem. Pharmacol.* **70**, 1267–1276.
86. Arias, H. R., Bhumireddy, P., Spitzmaul, G., Trudell, J. R., and Bouzat, C. (2006) Molecular mechanisms and binding site location for the noncompetitive antagonist crystal violet on nicotinic acetylcholine receptors. *Biochemistry* **45**, 2014–2026.
87. Samochocki, M., Höffle, A., Fehrenbacher, A., Jostock, R., Ludwig, J., Christner, C., Radina, M., Zerlin, M., Ullmer, C., Pereira, E. F., Lubbert, H., Albuquerque, E. X., and Maelicke, A. (2003) Galantamine is an allosterically potentiating ligand of neuronal nicotinic but not of muscarinic acetylcholine receptors. *J. Pharmacol. Exp. Ther.* **305**, 1024–1036.
88. Swanson, K. L. and Albuquerque, E. X. (1987) Nicotinic acetylcholine receptor ion channel blockade by cocaine: the mechanism of synaptic action. *J. Pharmacol. Exp. Ther.* **243**, 1202–1210.
89. Francis, M. M., Vazquez, R. W., Papke, R. L., and Oswald, R. E. (2000) Subtype-selective inhibition of neuronal nicotinic acetylcholine receptors by cocaine is determined by the  $\alpha$ 4 and  $\beta$ 4 subunits. *Mol. Pharmacol.* **58**, 109–119.
90. Hansen, S. B. and Taylor, P. (2007) Galanthamine and non-competitive inhibitor binding to ACh-binding protein: evidence for a binding site on non- $\alpha$ -subunit interfaces of heteromeric neuronal nicotinic receptors. *J. Mol. Biol.* **369**, 895–901.
91. Sine, S. M. and Engel, A. G. (2006) Recent advances in Cys-loop receptor structure and function. *Nature* **440**, 448–455.
92. Dutertre, S. and Lewis, R. J. (2006) Toxin insights into nicotinic acetylcholine receptors. *Biochem. Pharmacol.* **72**, 661–670.
93. Bafna, P. A., Purohit, P. G., and Auerbach, A. (2008) Gating at the mouth of the acetylcholine receptor channel: energetic consequences of mutations in the  $\alpha$ M2-cap. *PLoS ONE* **3**, e2515.
94. Zhou, Y., Pearson, J. E., and Auerbach, A. (2005)  $\Pi$ -value analysis of a linear, sequential reaction mechanism: theory and application to ion channel gating. *Biophys. J.* **89**, 3680–3685.
95. Purohit, P., Mitra, A., and Auerbach, A. (2007) A stepwise mechanism for acetylcholine receptor channel gating. *Nature* **446**, 930–933.
96. Grosman, C., Zhou, M., and Auerbach, A. (2000) Mapping the conformational wave of acetylcholine receptor channel gating. *Nature* **403**, 773–776.
97. Auerbach, A. (2005) Gating of acetylcholine receptor channels: Brownian motion across a broad transition state. *Proc. Natl. Acad. Sci. USA* **102**, 1408–1412.
98. Chakrapani, S., Bailey, T. D., and Auerbach, A. (2004) Gating dynamics of the acetylcholine receptor extracellular domain. *J. Gen. Physiol.* **123**, 341–356.
99. Mitra, A., Bailey, T. D., and Auerbach, A. L. (2004) Structural dynamics of the M4 transmembrane segment during acetylcholine receptor gating. *Structure* **12**, 1909–1918.
100. Cymes, G. D., Grosman, C., and Auerbach, A. (2002) Structure of the transition state of gating in the acetylcholine receptor channel pore: a  $\pi$ -value analysis. *Biochemistry* **41**, 5548–5555.
101. Lape, R., Colquhoun, D., and Sivilotti, L. G. (2008) On the nature of partial agonism in the nicotinic receptor superfamily. *Nature* **454**, 722–727.
102. Taly, A., Delarue, M., Grutter, T., Nilges, M., Le Novère, N., Corringer, P. J., and Changeux, J. P. (2005) Normal mode analysis suggests a quaternary twist model for the nicotinic receptor gating mechanism. *Biophys. J.* **88**, 3954–3965.
103. Taly, A., Corringer, P. J., Grutter, T., Prado de Carvalho, L., Karplus, M., and Changeux, J. P. (2006) Implications of the quaternary twist allosteric model for the physiology and pathology of nicotinic acetylcholine receptors. *Proc. Natl. Acad. Sci. USA* **103**, 16965–16970.
104. Amiri, S., Tai, K., Beckstein, O., Biggin, P. C., and Sansom, M. S. (2005) The  $\alpha$ 7 nicotinic acetylcholine receptor: molecular modelling, electrostatics, and energetics. *Mol. Membr. Biol.* **22**, 151–162.
105. Cheng, X., Lu, B., Grant, B., Law, R. J., and McCammon, J. A. (2006) Channel opening motion of  $\alpha$ 7 nicotinic acetylcholine receptor as suggested by normal mode analysis. *J. Mol. Biol.* **355**, 310–324.
106. Konstantakaki, M., Tzartos, S. J., Poulas, K., and Eliopoulos, E. (2008) Model of the extracellular domain of the human  $\alpha$ 7 nAChR based on the crystal structure of the mouse  $\alpha$ 1 nAChR extracellular domain. *J. Mol. Graph. Model.* **26**, 1333–1337.
107. Americ, S. P., Holladay, M., and Williams, M. (2007) Neuronal nicotinic receptors: a perspective on two decades of drug discovery research. *Biochem. Pharmacol.* **74**, 1092–1101.
108. Steensland, P., Simms, J. A., Holgate, J., Richards, J. K., and Bartlett, S. E. (2007) Varenicline, an  $\alpha$ 4 $\beta$ 2 nicotinic acetylcholine receptor partial agonist, selectively decreases ethanol consumption and seeking. *Proc. Natl. Acad. Sci. USA* **104**, 12518–12523.
109. Gotti, C., Riganti, L., Vailati, S., and Clementi, F. (2006) Brain neuronal nicotinic receptors as new targets for drug discovery. *Curr. Pharm. Des.* **12**, 407–428.
110. Miwa, J. M., Stevens, T. R., King, S. L., Caldarone, B. J., Ibanez-Tallon, I., Xiao, C., Fitzsimonds, R. M., Pavlides, C., Lester, H. A., Picciotto, M. R., and Heintz, N. (2006) The prototoxin lynx1 acts on nicotinic acetylcholine receptors to balance neuronal activity and survival in vivo. *Neuron* **51**, 587–600.
111. Ng, H. J., Whittemore, E. R., Tran, M. B., Hogenkamp, D. J., Broide, R. S., Johnstone, T. B., Zheng, L., Stevens, K. E., and Gee, K. W. (2007) Nootropic  $\alpha$ 7 nicotinic receptor allosteric modulator derived from GABAA receptor modulators. *Proc. Natl. Acad. Sci. USA* **104**, 8059–8064.
112. Timmermann, D. B., Gronlien, J. H., Kohlhaas, K. L., Nielsen, E. O., Dam, E., Jorgensen, T. D., Ahring, P. K., Peters, D., Holst, D., Christensen, J. K., Malysz, J., Briggs, C. A., Gopalakrishnan, M., and Olsen, G. M. (2007) An allosteric modulator of the  $\alpha$ 7 nicotinic acetylcholine receptor possessing cognition-enhancing properties in vivo. *J. Pharmacol. Exp. Ther.* **323**, 294–307.
113. Lloyd, G. K. and Williams, M. (2000) Neuronal nicotinic acetylcholine receptors as novel drug targets. *J. Pharmacol. Exp. Ther.* **292**, 461–467.
114. Poulas, K., Eliopoulos, E., Vatzaki, E., Navaza, J., Kontou, M., Oikonomakos, N., Acharya, K. R., and Tzartos, S. J. (2001) Crystal struc-

- ture of Fab198, an efficient protector of the acetylcholine receptor against myasthenogenic antibodies. *Eur. J. Biochem.* **268**, 3685–3693.
115. Kontou, M., Leonidas, D. D., Vatzaki, E. H., Tsantili, P., Mamalaki, A., Oikonomakos, N. G., Acharya, K. R., and Tzartos, S. J. (2000) The crystal structure of the Fab fragment of a rat monoclonal antibody against the main immunogenic region of the human muscle acetylcholine receptor. *Eur. J. Biochem.* **267**, 2389–2397.
116. Fostieri, E., Tzartos, S. J., Berrih-Aknin, S., Beeson, D., and Mamalaki, A. (2005) Isolation of potent human Fab fragments against a novel highly immunogenic region on human muscle acetylcholine receptor which protect the receptor from myasthenic autoantibodies. *Eur. J. Immunol.* **35**, 632–643.
117. Konstantakaki, M., Tzartos, S. J., Poulas, K., and Eliopoulos, E. (2007) Molecular modeling of the complex between *Torpedo* acetylcholine receptor and anti-MIR Fab198. *Biochem. Biophys. Res. Commun.* **356**, 569–575.
118. Bitzopoulou, K., Kostelidou, K., Poulas, K., and Tzartos, S. J. (2008) Mutant forms of the extracellular domain of the human acetylcholine receptor  $\gamma$ -subunit with improved solubility and enhanced antigenicity. The importance of the Cys-loop. *Biochim. Biophys. Acta* **1784**, 1226–1233.
119. Zouridakis, M., Zisimopoulou, P., Eliopoulos, E., Poulas, K., and Tzartos, S. J. (2008) Design and expression of human  $\alpha 7$  nicotinic acetylcholine receptor extracellular domain mutants with enhanced solubility and ligand-binding properties. *Biochim. Biophys. Acta*, in press.